Multiplicity and clustering in Taurus star-forming region

Isabelle Joncour, Gaspard Duchêne, Estelle Moraux

A&A 599, A14 (2017)
DOI: 10.1051/0004-6361/201629398

Astronomy & Astrophysics

Multiplicity and clustering in Taurus star-forming region

I. Unexpected ultra-wide pairs of high-order multiplicity in Taurus

Isabelle Joncour[1,2], Gaspard Duchêne[1,3], and Estelle Moraux[1]

[1] Univ. Grenoble Alpes, CNRS, IPAG, 38000 Grenoble, France
e-mail: isabelle.joncour@univ-grenoble-alpes.fr; joncouri@gaia.astro.umd.edu
[2] Department of Astronomy, University of Maryland, College Park, MD 20742, USA
[3] Astronomy Department, University of California, Berkeley, CA 94720-3411, USA

Received 26 July 2016 / Accepted 24 November 2016

ABSTRACT

Aims. This work analyses the spatial distribution of stars in Taurus with a specific focus on multiple stars and wide pairs in order to derive new constraints on star formation and early dynamical evolution scenarios.
Methods. We collected the multiplicity data of stars in Taurus to build an up-to-date stellar/multiplicity catalog. We first present a general study of nearest-neighbor statistics on spatial random distribution, comparing its analytical distribution and moments to those obtained from Monte Carlo samplings. We introduce the one-point correlation Ψ function to complement the pair correlation function and define the spatial regimes departing from randomness in Taurus. We then perform a set of statistical studies to characterize the binary regime that prevails in Taurus.
Results. The Ψ function in Taurus has a scale-free trend with a similar exponent as the correlation function at small scale. It extends almost 3 decades up to ∼60 kAU showing a potential extended wide binary regime. This was hidden in the correlation function due to the clustering pattern blending. Distinguishing two stellar populations, single stars versus multiple systems (separation ≤1 kAU), within Class II/III stars observed at high angular resolution, we highlight a major spatial neighborhood difference between the two populations using nearest-neighbor statistics. The multiple systems are three times more likely to have a distant companion within 10 kAU when compared to single stars. We show that this is due to the presence of most probable physical ultra-wide pairs (UWPs, defined as such from their mutual nearest neighbor property), that are themselves generally composed of multiple systems containing up to five stars altogether. More generally, our work highlights; 1) a new large population of candidate UWPs in Taurus within the range 1–60 kAU in Taurus and 2) the major local structural role they play up to 60 kAU. There are three different types of UWPs; either composed of two tight and comparatively massive stars (MM), by one single and one multiple (SM), or by two distant low-mass singles (SS) stars. These UWPs are biased towards high multiplicity and higher-stellar-mass components at shorter separations. The multiplicity fraction per ultra-wide pair with separation less than 10 kAU may be as high as 83.5 ± 19.6%.
Conclusions. We suggest that these young pre-main sequence UWPs may be pristine imprints of their spatial configuration at birth resulting from a cascade fragmentation scenario of the natal molecular core. They could be the older counterparts, at least for those separated by less than 10 kAU, to the ≤0.5 Myr prestellar cores/Class 0 multiple objects observed at radio/millimeter wavelengths.

Key words. open clusters and associations: individual: Taurus – stars: variables: T Tauri, Herbig Ae/Be – binaries: general – binaries: visual – methods: data analysis – stars: statistics

1. Introduction

The formation of stars results fundamentally from the runaway unbalance between overwhelming inwards self-gravity and outwards pressure-gradient forces (thermal, turbulence, magnetic, radiation, etc.) inside a perturbed gas cloud. Star formation has been known to be a complex process since at least the first model proposed almost three decades ago of a single isolated low-mass star formed out of one dense gas core (Shu et al. 1987). It also involves radiative processes (heating and cooling), generation and decay of turbulence and magnetic fields, chemical evolution of molecules, as well as dust and feedback mechanisms of newly formed stars in their natal environment. A realistic picture must be even more complicated since the stars are rarely born in isolation (Lada & Lada 2003) and, moreover, they are generally not single but part of multiple systems (Mathieu 1994; Duchêne & Kraus 2013). Overall, the whole story of star formation spans over ten orders of magnitude length-scale range. Giant gas clouds, having typical sizes from 10 pc to 100 pc (Dobbs et al. 2014), fragment, cool, and collapse to form dynamic clusters of young multiple objets whose sizes are approximately a solar radius. Since newly born stellar objects are closely linked to their gaseous progenitors (Hartmann 2002), their spatial distribution and their multiplicity properties offer important tests on star formation models.

Giant molecular clouds appear to be anything but uniform. They are highly substructured into a hierarchy of gas clumps and into highly intertwined filamentary networks, as strikingly revealed by the recent *Herschel* Gould Belt Survey (André et al. 2014). In turn these filaments shelter single or chains of molecular cores (Tafalla & Hacar 2015). Whether such heterogeneous patterns remain as the relics of the star formation processes in young stellar populations or are totally and quickly erased by subsequent dynamical evolution is an important question.

To seek such imprints of star formation, the giant Taurus molecular cloud is an ideal nursery. Its proximity (137 pc, Torres et al. 2007), the youth (1–10 Myr) of its stellar population

(Bertout et al. 2007; Andrews et al. 2013), and its low stellar density bring a complete census of approximately 350 young low-mass stars down to 0.02 $M_{\odot}$ (Luhman et al. 2010; Rebull et al. 2010). As there is a small spatial dispersion of (proto-)stars within the gaseous filament (Hartmann 2002; Covey et al. 2006), these stars are most probably born where they are now observed.

The current paradigm of star formation attributes a seemingly fundamental role to dense molecular cores thought to be the very cradles of stars (Ward-Thompson et al. 2007). The long-standing scenario proposed so far to form one low-mass star from one collapsing single core (Shu et al. 1987) predicts that the dense cores set the final mass of young stars. This is supported by the correspondence of the shapes of the core mass function (CMF) and the initial mass function (IMF) of stars, although the peak of the IMF is shifted by a factor 2–3 towards lower mass. This shift may be due to a partial 30–40% efficiency gas to star conversion (Alves et al. 2007; Lada et al. 2008; Marsh et al. 2016; Könyves et al. 2015), although this estimate is higher than the star-formation efficiency (1–10%) estimated for the whole cloud. Alternatively, such a shift between the core mass function and the initial mass function may also result from the multiplicity of stars born within one individual core that has undergone multiple fragmentation (Goodwin et al. 2008). This may lead to a core-to-stars efficiency as high as 100% (Holman et al. 2013; see for a review Offner et al. 2014).

The multiplicity appears to be a key feature in star-forming regions. The companion frequency of young stars in Taurus is generally twice that of field stars (Duchêne & Kraus 2013), and the formation of coeval and wide binaries up to 5 kAU is a common outcome of the star formation process (Kraus & Hillenbrand 2009a). Furthermore, since multiplicity appears to decrease with age (see for a review Duchêne & Kraus 2013) due to dynamical evolution, observing multiplicity at this young age means that the multiple system-core picture of star formation is the rule rather than the exception. In this picture, the maximal size of multiple systems cannot exceed the size of their progenitor cores, typically approximately 20 kAU, that is, 0.1 pc (Ward-Thompson et al. 2007). If the dense cores are de facto the smallest bricks to build a young stellar population, we then expect that spacing between stars as well as binary semi-major axes be related to parental molecular core size and spacing, provided that dynamical evolution has not erased early imprints. Furthermore, if the formation of multiple systems and single stars share a common scenario, we do not a priori expect any difference in spatial distribution between the two.

Several spatial studies have been performed in Taurus. Some were based on the stellar two-point correlation function and the related mean surface density of companions to examine the scale-free behavior of clustering modes (Gomez et al. 1993; Larson 1995; Simon 1997; Gladwin et al. 1999; Hartmann 2002; Kraus & Hillenbrand 2008). Other studies based on first-nearest-neighbor separation (1-NNS) statistics analysis aimed either at comparing the spatial distribution of stars in Taurus to a random distribution (Gomez et al. 1993) or at studying their distribution as a function of their mass and spectral energy distribution (SED) (Luhman 2006; Luhman et al. 2010).

In this work, after a description of the stellar data catalog we have built to perform our studies (Sect. 2), we apply these two statistical tools (1-NNS distribution and two-point correlation function) to analyse the spatial distribution of stars in Taurus with a focus on multiples with respect to single stars, while introducing the one-point correlation function Ψ (Sect. 3). We then assess the statistical properties of 1-NNS couples while defining ultra-wide pairs (UWP) as mutual nearest neighbors in the range of 1–100 kAU and we show the crucial role they play in spatial clustering features (Sect. 4). We make a synthesis of results and open a discussion (Sect. 5) before a summary to conclude the paper (Sect. 6).

2. Data

2.1. Input catalog

Although a recent catalog of Taurus members has been released including newly detected mid-infrared Wide-field Infrared Survey Explorer (WISE) sources (Esplin et al. 2014), we adopted the catalog containing 352 Taurus members that offers a full census of members down to 0.02 $M_{\odot}$ (Luhman et al. 2010; Rebull et al. 2010), which we supplemented with stellar multiplicity data. The newly identified WISE members are mainly due to a wider coverage of the Taurus region compared to *Spitzer*'s, similar to the new candidates recently identified in Taurus using the Sloan Digital Sky Survey (Luhman et al. 2017). These new members belong primarily to the dispersed stellar population and have typically not been observed at high angular resolution (HAR), hence multiplicity information is not complete for these sources. Therefore, setting this population aside should not significantly affect our conclusions surrounding local pairing statistical properties. Moreover, the Luhman et al. (2010) catalog provides a full and coherent analysis of SEDs as obtained from the *Spitzer* Infrared Array Camera and Multiband Imaging Photometer, leading to a system of four Classes of SED (Class 0, I, II, and III objects) that we will use in our statistical studies. This classification is widely used to assess the evolutionary state of the material surrounding the star (Lada & Wilking 1984; Lada 1987; Andre et al. 1993; Greene et al. 1994). Further studies have revealed that pure SED analyses can be misleading (Carney et al. 2016) for individual objects. However, although uncertainties remain on the individual classification, there is a clear statistical sequence of ages as a function of SED classification when the population is taken as an ensemble.

Taurus is known to be the archetype of low-mass star formation in loose groups (Jones & Herbig 1979; Gomez et al. 1993; Kirk & Myers 2011). The star mass estimates were taken from the latter work exploiting the same catalog of stars from Luhman et al. (2010). We note that the stellar masses have been estimated from their spectral type while assuming a constant age of 1–2 Myr for all stars of the complex and using an ad hoc isochrone at 1–2 Myr composed of a sequence of several theoretical evolutionary tracks depending on the mass range (see Kirk & Myers 2011, for details). Since a recent careful analysis based on optical spectroscopic study of young stars in star-forming regions, including Taurus, has shown that spectral types measured over the past decade are mostly consistent with the new evaluation (Herczeg & Hillenbrand 2014), the main source of uncertainties surrounding mass estimation comes from the hypothesis of a unique age for all the members (1–2 Myr).

The mass was estimated for each star using the effective temperature converted from its spectral type and an ad-hoc isochrone at 1–2 Myr composed of a sequence of several theoretical evolutionary tracks depending on the mass range (see Kirk & Myers 2011, for details). For a given spectral type, assuming a younger age for a star than reality will tend to underestimate its mass. But, even if the absolute value of the mass is subject to great uncertainties (30 to 50%), yet we do not expect a systematic differential bias in mass estimation. Besides, there is no indication of a mixture of components in the age distribution that would suggest

the presence of distinct episodic generation of stars, nor any evidence of a systemic dynamical evolution that would divide the stars into distinct age-based populations. New generation of stars and dynamical evolution appear to be continuous processes that globally lead to a smooth dispersion of age. For instance, multiple systems and single stars have a same mean age and display the same age dispersion (White & Ghez 2001). Thus, assuming a single age for all the stars will bias the absolute value of each derived mass, but the relative difference between them, which is used in our analysis, should be much less affected.

2.2. Multiplicity

To construct a census of stellar systems in Taurus, we began by compiling a list of all known multiple members of the region from almost three decades of increasingly higher-angular-resolution observations (see references in Table C.1). We also assigned a flag to each star when it has been observed at HAR.

In order to separately study the populations of single stars and multiple systems and to distinguish clustering from multiplicity, we grouped together all stars that are separated by less than 7″ (0.92 kAU ∼ 1 kAU) to form a single entity. Throughout this paper we refer to them simply as "multiple systems". This threshold is, to a certain extent, arbitrary. However, two reasons motivate this choice. First of all, it is the lower threshold that defines wide binaries (separation >1 kAU) and secondly (the main reason), this threshold is close to the 6″ beam of the *Spitzer*-MIPS data. Thus, we ensure that the census of neighbor stars beyond 1 kAU is completely independent of the Class of the Taurus members.

We assigned the total number of stars within a 1 kAU radius n_* (for a single star $n_* = 1$, for a binary $n_* = 2$, ...) to each entry of the catalog, and we note that this parameter is only reliable for Class II and III type stars that have been observed at HAR, using techniques such as speckle interferometry imaging and adaptive optics with spatial resolution between 0.05″ to 2″. These techniques probe the immediate neighborhood of a star, at least beyond ∼10 AU at the distance of Taurus (i.e., 5−20 AU depending on the technique). Very close binaries (i.e., $\lesssim$10 AU) most probably originate from a distinct scenario from other binaries, as they are probably not formed by fragmentation in situ (Bate et al. 2003). We thus consider spectroscopic binaries and the closest visual binaries (below ∼20 AU) as single stars to ensure the consistency and completeness of our visual binary analysis, since no exhaustive spectroscopic binaries survey has been performed till now.

The resulting catalog (see Table C.1) contains 338 sources. Of these, 250 have been observed at HAR and amongst the latter 94 are multiple systems, resulting in a mean multiplicity fraction (MF) of 40%, which could truly be as high as 54%, if all the remaining stars that have not been observed at HAR are multiple systems. A similar multiplicity fraction is obtained when considering only Class II/III stars (i.e., MF = 40% ± 10%). The mean companion frequency for Class II/III stars observed at HAR is 48%. We note that a chi-squared test shows that the proportion of Class I, II, and III in the star sample observed at HAR is statistically the same when considering either single stars or multiple stars. The disk fraction (the number of Class II stars over the number of Class II and III stars) is also statistically the same in the two populations. Using Class as a proxy for the age, we obtain, as already stated by White & Ghez (2001) that uses theoretical stellar evolution models, that the two populations share the same age and the same range of age dispersion.

Table 1. Sub-samples of stars in Taurus.

Sub-sample	Spatial region	Class	HAR	N
$S1$	whole	All	No	338
$S2$	$W_{\rm in}$	All	No	252
$S3$	whole	II, III	Yes	179

Notes. Sub-samples of our star catalog depending on their spatial location (whole region of Taurus or within $W_{\rm in}$, see Fig. 1), their Class, or whether or not they all have been observed at HAR. N: total numbers of stars within the sub-sample.

2.3. Samples

The sources in Taurus, as was first pointed out by Gomez et al. (1993), are not randomly distributed on the sky (see Fig. 1). Some sets of stars appear grouped at a global scale in two structures located North (in L1507 molecular cloud) and South-West (in L1543 molecular cloud) with respect to the three main filaments, while some of them are tightly subgrouped at small scales within the main central filaments. Yet, other stars appear more spatially dispersed between the main structures. One of the goals of this work is to more precisely quantify their spatial distribution based on nearest-neighbor analysis, now that the census of star population in Taurus has more than doubled since the seminal work of Gomez et al. (1993).

From our catalog we extracted three distinct samples (defined in Table 1) that we use to test different hypotheses throughout this work, notably for multiplicity testing.

3. Local spatial analysis

In this section, we perform the spatial analysis of stars in the entire Taurus region and we assess the difference in the spatial distribution between multiple systems and single stars based on their respective first nearest neighbor separation (1-NNS) statistics. Nearest-neighbor statistics have been used for decades in Taurus to; (1) demonstrate departures from random uniform distributions (Gomez et al. 1993); (2) show that the spatial distribution of brown dwarfs and stars are undistinguishable (Luhman 2004); and (3) study the spatial distribution of stars as a function of their Class (Luhman et al. 2010). We start with some preliminary work on 1-NNS statistics to advocate the use of the theoretical 1-NNS distribution derived for a random distribution in an infinite medium as a reliable proxy for a random distribution enclosed in a finite and irregularly shaped window provided that the window is large and well-populated. We then define the one-point correlation function Ψ, which complements the two-point correlation function, to study the binary regime. This function allows us to quantify the departure of a population from a random uniform one and to identify distinct spatial regimes (clustering, inhibition, and dispersion).

Most of our work was performed using the free R software environment for statistical computing and graphics (R Core Team 2015) using a set of packages such as *Spatstat, Hmisc, fields, FITSio, calibrate, xtable, astrolab, deming, mixtools,* and *magicaxis* (Baddeley & Turner 2005; Harrell et al. 2015; Nychka et al. 2015; Harris 2013; Graffelman 2013; Dahl 2014; Chakraborty et al. 2014; Therneau 2014; Benaglia et al. 2009; Robotham 2015).

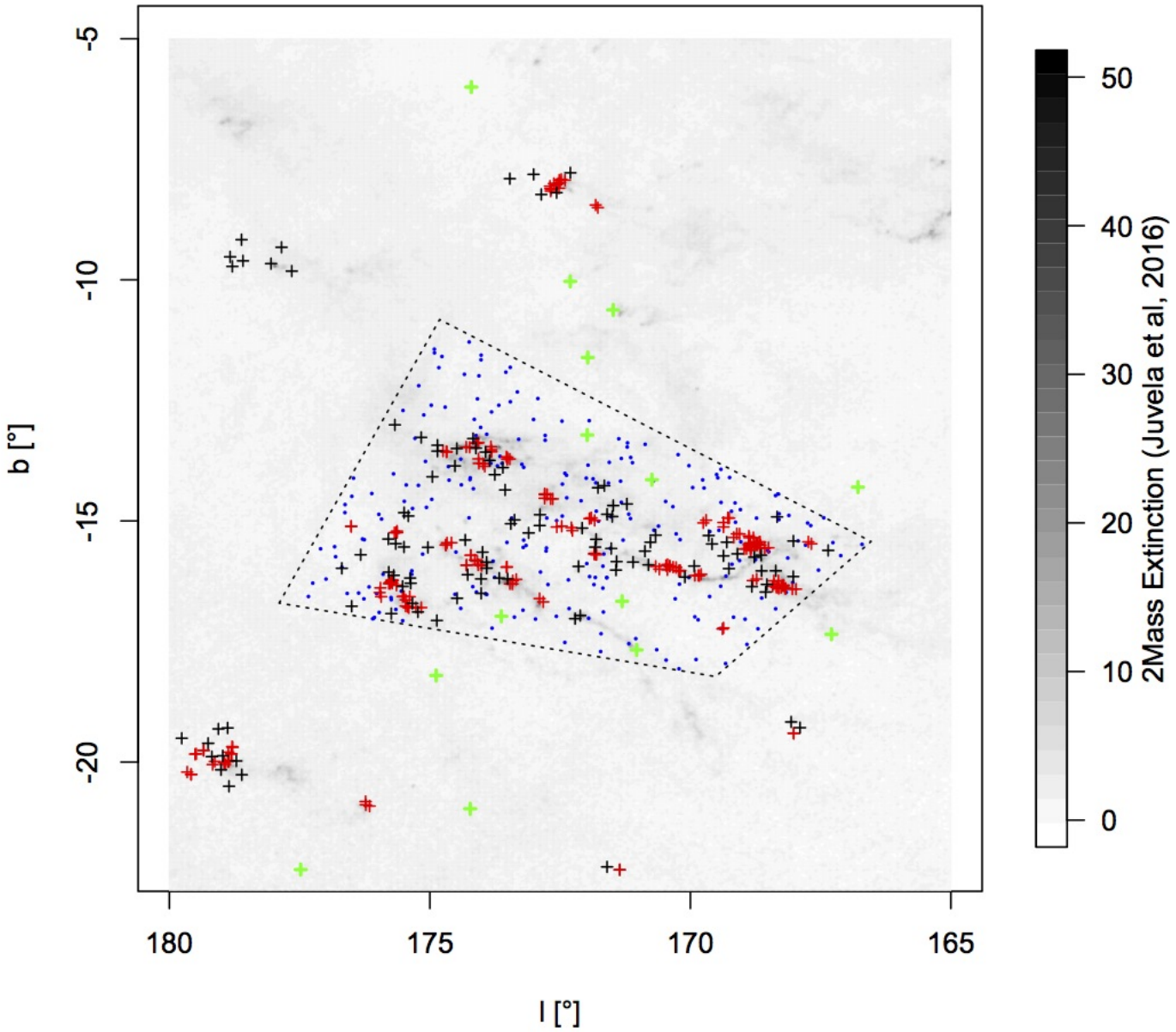

Fig. 1. Spatial distribution of stars within the Taurus region superimposed on near-infrared extinction (unit mag, gray scale) from Juvela & Montillaud (2016). Dashed polygon: restricted spatial window W_{in} in Taurus complex; blue filled dots: random sampling. Color-coding for Taurus stars: red plus marks: clustered stars [1-NNS $\leq 0.1°$]; black plus marks: "inhibited" regime stars [$0.1° <$ 1-NNS $\leq 0.55°$]; green plus marks: isolated stars [1-NNS beyond 0.55°] (see Sect. 3).

3.1. 1-NNS study in Taurus

This subsection aims at analyzing the spatial distribution in Taurus based on a 1-NNS analysis. The 1-NNS of a star is, by definition, the distance to its nearest neighbor star. Throughout this paper, we deal with the projected 1-NNS, computed for each star as the minimum value of projected angular distance between each pair of stars onto the celestial sphere (see Appendix A).

After estimating the mean surface density of stars, we first compare the Taurus 1-NNS distribution in the three main filaments to that associated to the entire region. We then compare the theoretical random 1-NNS distribution obtained for an infinite random spatial process to the 1-NNS distribution derived from Monte Carlo samplings in a finite irregularly shaped window, and finally we compare Taurus 1-NNS distribution to the 1-NNS random distribution.

3.1.1. Mean stellar surface density in Taurus

To derive an estimate of the mean surface density ρ_w of the spatial process in Taurus, we focus on its central part as the least heterogeneous area and define the spatial polygonal window W_{in} that encloses the central three main filaments (see Fig. 1), to get:

$$\rho_w = N_w/A_w \sim 5 \text{ deg}^{-2} \sim 1 \text{ pc}^{-2}, \quad (1)$$

where $A_w = 48.5 \text{ deg}^2$ (i.e. 289.57 pc^2) is the projected area of the window W_{in} that encloses $N_w = 252$ stars. This window defines our star sample S_2 (see Table 1).

In the following paragraph, we estimate the uncertainty of the mean projected stellar surface density of Taurus. A conservative estimate of the uncertainty on the surface density may be obtained when choosing for the window, the convex hull of the stars enclosed within the polygonal window W_{in}. The convex hull of

Table 2. Moments of the 1-NNS distribution in Taurus.

Spatial window	Stars sample	$\bar{r}$ [pc]	$r_{0.5}$ [pc]	σ^2 [pc^2]	σ [pc]	γ
whole region Taurus	S_1	0.38 ± 0.04	0.17 ± 0.06	0.55 ± 0.05	0.74 ± 0.03	5.91 ± 0.32
$W_{\rm in}$ Taurus	S_2	0.28 ± 0.02	0.16 ± 0.03	0.14 ± 0.01	0.37 ± 0.02	3.18 ± 0.19
Infinite	Rand. Theo	0.54	0.50	0.08	0.28	0.63
$W_{\rm in}$	Rand. MC	0.55 ± 0.02	0.51 ± 0.02	0.09 ± 0.01	0.30 ± 0.01	0.84 ± 0.05

Notes. The moments of the 1-NNS distribution are given for: all stars in the whole Taurus region (sample S_1, see Table 1), stars within the $W_{\rm in}$ window (sample S_2, see Table 1 and Fig. 1), the random theoretical 1-NNS distribution "Rand. Theo" in an infinite medium $w_R(r) = 2\pi\rho r \exp(-\pi\rho r^2)$ (Eq. (B.1)), and the 1-NNS distribution obtained from the 10 000 random Monte Carlo samplings "Rand. MC" within the $W_{\rm in}$ window. The two random distributions are computed using the same intensity process $\rho = 5$ deg^{-2} (see Eq. (1)). The uncertainties are evaluated from Eq. (5), with $N = 252$.

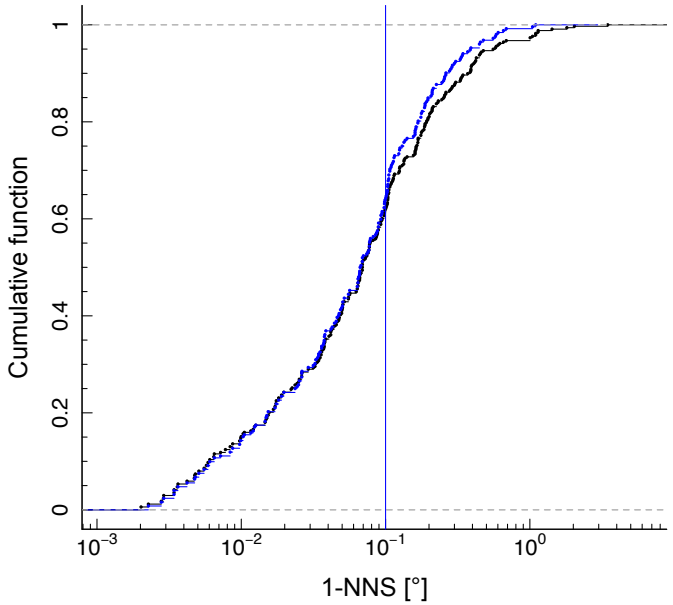

Fig. 2. Empirical cumulative distribution of the 1-NNS distribution for the whole region (black) and for the central part within $W_{\rm in}$ region (blue). The blue vertical line represents the clustering length, $r_c = 0.1°$.

a set of points in the Euclidean space is defined as the smallest convex set of points that contains the whole set of points.The area of the convex hull, $A \sim 33$ deg^2, being less than the polygonal window, the surface density estimate mechanically increases by a factor of 1.6 ($N_w/A \sim 8$ deg^{-2}). Conversely, taking the convex hull area of the whole Taurus region (∼202 deg^2) containing 338 objects lowers the mean surface density to ∼2 deg^{-2}. Combined, these extreme cases yield a probable range for the projected stellar density of Taurus of

$$\rho \sim 5 \pm 3 \,\text{stars/deg}^{-2}. \quad (2)$$

3.1.2. 1-NNS distribution across Taurus

The 1-NNS median value evaluated within the full region of Taurus (see Table 2) does not differ from the 1-NNS median value evaluated within the three main filaments, and their 1-NNS cumulative distributions do not differ either for length scale below $r_c \sim 0.1°$ (see Fig. 2). This indicates that the spatial properties of the spatial distribution of stars are similar across the whole region of Taurus below this angular scale. Above the 0.1° scale, the two cumulative distributions diverge due to the presence of highly dispersed stars between the three main filaments and other main stellar concentrations in Taurus. As a result of these, the 1-NNS distribution of the whole region has a more populated large-scale tail. Nonetheless, up to the third quantile, the 1-NNS quartiles are similar. As a matter of fact, due to its highly asymmetrical shape, the Taurus 1-NNS distribution is better evaluated using quantiles rather than the mean and standard deviation that are more conveniently suited for symmetrical functions.

3.1.3. 1-NNS distribution: theoretical random vs. Monte Carlo samplings

In this subsection, we compare the theoretical 1-NNS distribution for a spatially random process in an infinite media to the 1-NNS distribution obtained from Monte Carlo samplings in a finite, irregularly-shaped window to establish that the former can be used as a reliable proxy for the latter.

The random theoretical 1-NNS distribution $w_R(\log r)$ derived for an infinite media (see Appendix B for the full development) is given by:

$$w_R(\log r) = 2\,\ln(10)\,\pi\,\rho\,r^2\,\exp(-\pi\rho r^2), \quad (3)$$

where ρ is the mean intensity of the random process (the average surface density of stars) and r is the 1-NNS. We want to compare this theoretical distribution to the 1-NNS histogram obtained from 10 000 random Monte Carlo samplings within the finite and irregularly-shaped window $W_{\rm in}$ (see Fig. 3). Their respective moments are similar (see Table 2), with theoretical moments computed from the following expressions:

$$\bar{r} \simeq 1/(2\sqrt{\rho}), \quad (4a)$$

$$\sigma^2 = (4-\pi)(4\pi\rho)^{-1}, \quad (4b)$$

$$\gamma = 2\sqrt{\pi}(\pi-3)/(4-\pi)^{3/2}, \quad (4c)$$

$$r_{0.5} = \sqrt{\ln 2/(\pi\rho)}, \quad (4d)$$

where $\bar{r}$, $r_{0.5}$, σ^2, σ^2, and γ are the mean, median, variance, standard deviation, and skewness factor (see Appendix B for their derivation). The moments from random Monte Carlo samplings

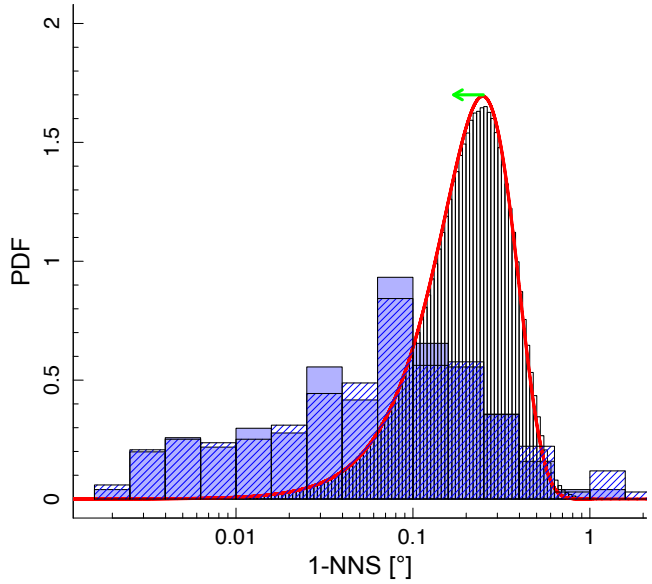

Fig. 3. Probability distribution function (PDF) of the 1-NNS distributions observed in Taurus (solid blue histogram: within the limited window $W_{\rm in}$, that is, the three main filaments; dashed blue histogram: the entire Taurus region) and predicted for a random distribution (black histogram: for a Monte Carlo sampling within the window $W_{\rm in}$; red curve: unlimited theoretical random 1-NNS distribution, see Eq. (3)). Both random populations are drawn using the same mean surface density $\rho_{\rm w} = 5\,{\rm deg}^2$. Increasing the mean density by a factor of two leads to a shift towards the left whose amplitude is represented by the green arrow. The Monte Carlo sampling in a finite window and the unlimited theoretical random 1-NNS do not significantly differ. The 1-NNS distributions computed either in the whole Taurus or within $W_{\rm in}$ do not significantly differ either. However, the Taurus and random 1-NNS distributions are statistically highly inconsistent, with a p-value of $\sim 10^{-16}$ for the KS test. The spatial distribution in Taurus is clearly far from being random.

were obtained from:

$$\overline{r} = \frac{1}{N-1}\sum_{1}^{N} r_i \pm [N_i - 1]^{-1/2}\ \sigma_{\rm Tau},$$

$$\sigma^2 = \frac{1}{(N-1)}\sum_{1}^{N}(r_i - \overline{r})^2 \pm \sqrt{2}\,[N-1]^{-1/2}\,\sigma^2,$$

$$\sigma = \sqrt{\frac{1}{N-1}\sum_{1}^{N}(r_i - \overline{r})^2} \pm [2\,(N-1)]^{-1/2}\,\sigma,$$

$$\gamma = \frac{N}{((N-1)(N-2))}\sum_{1}^{N}(r_i - \overline{r})^3 \pm (N-1)^{-1/2}\,\gamma,$$

$$r_{0.5} = \Lambda_{0.5} \pm \sigma\sqrt{\pi/(2(N-1))} \qquad (5)$$

where Λ is the ordered sequence of the 1-NNS from the smallest to the highest value, the standard errors of the moments and the standard error of the median are taken respectively from Ahn & Fessler (2003) and Kendall & Stuart (1977).

We thus conclude that finite size and edge window effects do not significantly alter the distribution of 1-NNS from that obtained in an infinite medium at the level of our observational uncertainties. To prove this statement quantitatively, we use a bootstrapping technique, comparing 10 000 realizations of a) a sample of $N \sim N_{\rm w} = 252$ 1-NNS obtained from standard rejection sampling technique using analytical random 1-NNS distribution (Eq. (3)) to b) the 1-NNS associated to random Monte Carlo samplings of 252 stars enclosed within $W_{\rm in}$. The two-sample Kolmogorov-Smirnov (KS) and Anderson-Darling (AD) statistical tests indicate that the two 1-NNS distributions cannot be statistically distinguished with a mean p-value and standard deviation respectively of 0.36 ± 0.28 for the KS test and 0.34 ± 0.27 for the AD test.

We have therefore shown that the random theoretical 1-NNS probability density function (Eq. (3)) may be used as a reliable proxy to describe a 1-NNS random distribution even in the case of a random population enclosed in a finite and irregularly shaped window, such as $W_{\rm in}$. We mention, as an asset, that using random theoretical 1-NNS distribution proxy avoids large Monte Carlo sampling computations required to populate highly improbable bins of very small spacings associated with tightly clustered regions.

3.1.4. Spatial distribution in Taurus

The comparison between the Taurus and random 1-NNS distributions clearly reveals an excess of short spacings in Taurus (see Fig. 3), for which the 1-NNS distribution has smaller central values (median and mean) and a wider dispersion (see Table 2). The 2-sample KS and AD tests, give a p-value less than $\leq 2.2 \times 10^{-16}$ and $\leq 10^{-40}$, respectively, that the two samples are mutually consistent. Thus, we can firmly reject the hypothesis that the spatial distribution of stars within Taurus is random.

This result is not surprising, since the same conclusion was already reached by Gomez et al. (1993) based on a sample of 139 stars. But the expansion of the stellar census by nearly 200 new stars in Taurus strengthens this conclusion. The median value of the 1-NNS distribution we derived is $r_{0.5} \sim 0.067°$ (~0.16 pc, i.e. 33 kAU); almost half the value obtained by these authors. This is what we expect when the spatial distribution of additional stars follows a similar spatial pattern from the original population, since from Eq. (4d), the median value is reduced by a factor of $\sim\sqrt{338/139} \sim 1.5$.

This also underlines the modest usefulness of the absolute value of the median nearest-neighbor distance to determine clustering property when the stellar census is incomplete. In the following section, we introduce an alternative criterion based on the one-point correlation function to quantitatively assess local departures from pure randomness and to determine characteristic clustering scales.

3.2. One and two-point correlation statistics

In order to identify a criterion that quantifies the departure of a spatial distribution of stars from randomness, we introduce the one-point correlation function based on the 1-NNS distribution. This function is a new tool to assess and quantify the binary and spatial clustering regimes of stars and aims at complementing the two-point correlation statistics.

3.2.1. The two-point and pair correlation functions

The two-point correlation function (TPCF) $\xi_V(\boldsymbol{r})$ is defined for a 3D spatial process as a measure of the probability to get any excess of stellar pairs with a separation distance vector $\boldsymbol{r}$ above random expectation: $dP = \rho_V^2(1 + \xi_V(\boldsymbol{r}))dV_1 dV_2$, where ρ_V is the mean volumic density of the uniform random process and dP is

the infinitesimal joint probability to find a pair of stars respectively centered in the volume elements dV_1 and dV_2 and separated by $\boldsymbol{r}$ (Peebles 1980). Similarly, for an isotropic and stationary spatial process, the standard projected angular two-point correlation function $\xi(r)$ is then defined as the probability to find a pair of stars each separated by a projected angular distance r above random expectation: $dP = \rho^2(1 + \xi(r))d\Omega_1 d\Omega_2$, where ρ is the density of stars per steradian and dP is the infinitesimal joint probability to find a pair of stars each within a unit solid angle $d\Omega_1$, $d\Omega_2$ and separated by a projected angular distance r.

Besides the two-point correlation function, the second order statistics may also be evaluated from related entities:

- the main surface density of companions (MSDC) above random expectation: $\Sigma(r) = \rho\xi(r)$;
- the pair correlation function $g(r)$ as a measure of the probability to have any pair of stars separated by r: $g(r) = 1 + \xi(r)$.

When the spatial distribution is random, all these functions are constant ($\xi(r) = 0, g(r) = 1, \Sigma(r) = 0$). Although different estimators may be used to compute the pair correlation function (Landy & Szalay 1993; Kerscher et al. 2000), we use the simple and natural one defined as:

$$\hat{g}(r) = \frac{N_{\rm Tau}^{\rm Pairs}(r)}{N_{\rm R}^{\rm Pairs}(r)}, \tag{6}$$

where $N_{\rm Tau}^{\rm Pairs}(r)$ and $N_{\rm R}^{\rm Pairs}(r)$ are the histogram of separations between stars within Taurus and in a randomly distributed catalogue, respectively.

Since the pair correlation function estimate is mainly sensitive to the shape and extension of the window, no straightforward theoretical expression can be derived for $N_{\rm R}^{\rm Pairs}(r)$ on general grounds, even in the random spatial distribution case. We then compute the pair correlation function using Eq. (6) while performing 100 000 random Monte Carlo samplings within $W_{\rm in}$ (see Fig. 4).

The slope and the shape of the resulting Taurus pair correlation fonction are comparable to those obtained in previous works studying the two-point correlation function or the main surface density of companions (Gomez et al. 1993; Larson 1995; Simon 1997; Gladwin et al. 1999; Hartmann 2002; Kraus & Hillenbrand 2008). Together with our own, these studies show that the second order statistics exhibit at least two distinct power-laws: a steep binary/multiple regime at small scale and a smoother clustering regime beyond a breaking point. Larson (1995) suggested that; (1) the observed break at 0.04 pc (8.25 kAU) can be the signature of the transition from a binary to a clustering regime; (2) it could correspond to the Jeans length for the gas in cool dense molecular cores; (3) the scale-free binary regime may reflect the scale-free fragmentation of collapsing clumps; and (4) the self-similar clustering regime may reflect the hierarchical, fractal, and spatial distribution of the gas from which the stars formed.

Later on, Kraus & Hillenbrand (2008) found an extended transition zone between the binary regime and the global clustering of stars in groups rather than a sharp break between the two regimes. This transition zone was found to begin at 0.02 pc (4.25 kAU) and end at 0.2 pc (42.5 kAU). They proposed that part of this transition zone, which is almost flat from 0.11 pc (23.52 kAU) to 0.2 pc (42.5 kAU), is due to the random motion of stars that may smooth out primordial stellar association and lead to a quasi-constant surface density of pairs.

However, some caution has to be taken when interpreting the two-point correlation function beyond the binary regime, especially when the spatial distribution of stars deviates from isotropy. Indeed the standard form of the two-point correlation function is obtained with the hypothesis of a homogeneous and isotropic distribution. However, the Taurus complex is not isotropic, as evidenced by its elongated gaseous structures in which stars are preferentially located. The break in the two-point correlation function between the binary and the clustering regimes may thus be partly due to the filamentary geometrical anisotropy, rather than being only a signature of a hierarchical/fractal gas structure as proposed by Larson (1995).

Indeed, the observed break in the two-point correlation function could also be linked to the observed width of filaments, which was found to be relatively universal at approximately 0.1 pc (André et al. 2014) even though Ysard et al. (2013) found that filament width may vary by up to a factor of approximately four. This spread of filament widths may also contribute to the transition elbow zone that is present between the binary and clustering regimes. Thus, the elbow in the correlation function that extends up to 0.25 pc may be related to geometrical spatial stellar structures (see Joncour et al., in prep.).

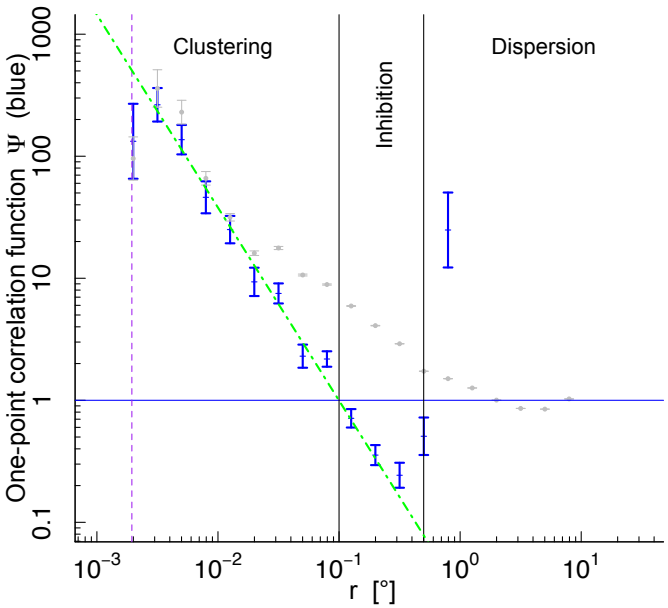

Fig. 4. One-point correlation function Ψ (Eq. (7), blue symbols) and estimated pair correlation function g (gray symbols) using the sample of stars within $W_{\rm in}$. The pair correlation function has been estimated using the estimator given in Eq. (6) while performing 10 000 random Monte Carlo samplings within $W_{\rm in}$. The 1σ vertical errorbars of Ψ and g are estimated from Poisson statistics. The solid horizontal blue line represents both the constant $\Psi = 1$ and $\hat{g} = 1$ functions, that is, the one-point and pair correlation function expected for a spatial random distribution. Vertical black solid lines delimit three spatial regimes, clustering, inhibition, and dispersion, derived from the crossing of the Taurus Ψ function with the $\Psi = 1$ horizontal line associated to random spatial distribution. The vertical dashed purple line indicates the 7″ spacing threshold used to group stars into a unique multiple system. The dotted-dashed green line is the $\Psi \propto r^{-1.5}$ function resulting from a linear regression fit taking into account vertical errorbars over ten 1-NNS logarithm bins ($\Delta \log r = 0.2$). The Ψ function may reveal an extended binary regime from 1.6 kAU to 100 kAU in Taurus, which has remained unidentified beyond approximately 5 kAU in previous works that used the pair correlation function alone, since the latter reveals a power law break around that separation.

3.2.2. The one-point correlation function

Similarly to the pair correlation function, we define the one-point correlation function, Ψ, as the probability of having a closest star located at r from any chosen star at random, which in turn defines an equivalent local stellar density function σ: $\mathrm{d}P = \sigma(r)\mathrm{d}V$, with $\sigma(r) = \rho\Psi(r)$. The Ψ function, which describes the spatial location of stars, gives first order variation trends of the spatial process relative to a random distribution. Instead, the pair correlation function is associated to second-order characteristics describing the spatial co-location of stars. One estimator of the Ψ function may be defined from the ratio of the 1-NNS Taurus distribution $w_{\mathrm{Tau}}(\log r)$ to the 1-NNS random distribution $w_R(\log r)$ obtained either by Monte Carlo simulations or from theoretical random probability density function (Eq. (3)):

$$\Psi(\log r) = \frac{w_{\mathrm{Tau}}(\log r)}{w_R(\log r)}. \quad (7)$$

We note that this function is usually called the nearest neighbor ratio when it is evaluated as the average over the whole range of 1-NNS values. Here we evaluate it bin per bin of spacing. For a random spatial distribution, the one-point correlation function reduces to unity ($\Psi(r) = 1$).

The one-point correlation Ψ function can be fitted from 1.6 kAU to ~100 kAU, by a power law using Pearson's chi-squared linear regression taking into account vertical errorbars (see Fig. 4):

$$\Psi = \frac{w_{\mathrm{Tau}}}{w_R} \propto r^{-\alpha}, \quad (8)$$

with $\alpha = 1.5^{+0.2}_{0.3}$ at the 95% confidence level. This allows us to derive a fractal dimension D_{f} associated to the binary regime in Taurus. Since the random distribution in 2D increases as $w_R \propto r^2$ for $r \ll 1/\sqrt{\pi\rho}$ (see Appendix B), the 1-NNS distribution within Taurus w_{Tau} follows a shallow, rising power-law function with the following exponent:

$$D_{\mathrm{f}} \sim 2 - \alpha = 0.5. \quad (9)$$

We note, that this scale-free behavior of the Ψ function with an exponent lower than the projected 2D euclidian space dimension is equivalent to a uniform distribution in a 2D projected fractal space with the fractal dimension $D_{\mathrm{f}} = 0.5$ (Sakhr & Nieminen 2006).

3.2.3. Departure from randomness

The one point correlation function Ψ may be used to assess departure from a spatially random distribution. From its definition, regimes where Ψ is below unity indicate a deficit of stars (inhibition) with respect to random, whereas where it is above unity reveals an excess of stars, either a clustering trend at small spacings (aggregation) or a dispersion trend at large spacings. The Ψ function evaluated for Taurus thus reveals three spatial regimes (see Fig. 4). The stellar clustering regime covers the range of spacings below ~0.1°, where $\Psi(r) > 1$. This defines the upper clustering length threshold r_{c}:

$$r_{\mathrm{c}} = 0.1^\circ \sim 0.24\,\mathrm{pc} \sim 50\,\mathrm{kAU}. \quad (10)$$

The clustering regime is followed by an "inhibition zone" where $\Psi(r) < 1$ associated with a typical length scale between ~0.1° (0.2 pc) and ~0.3° (0.7 pc). Finally, Taurus faces an excess of highly dispersed stars for typical length scale above ~0.3°. The "clustered stars" are tightly packed together in specific locations while the "inhibited stars" are more widely spread between the zones of clustered stars (see Fig. 1).

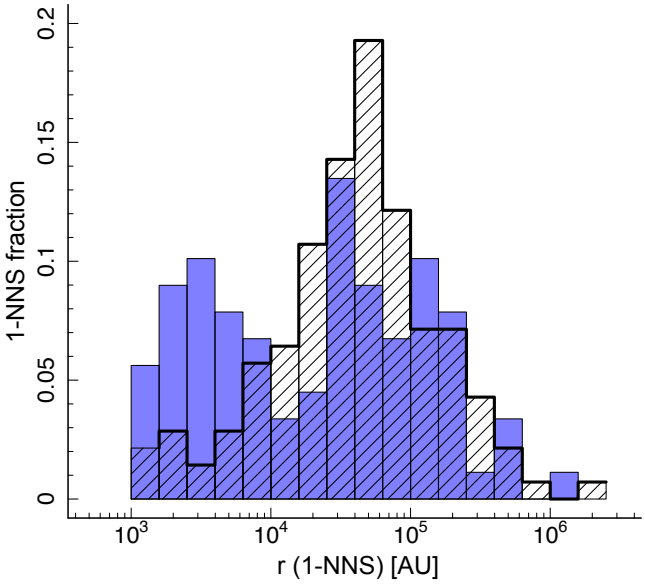

Fig. 5. First nearest neighbor separation fraction distribution of multiple systems (solid blue histogram) versus single stars (dashed black histogram) for Class II and III objects observed at high angular resolution (HAR) in Taurus region. Each bin represents the number density of stars per unit logarithmic interval in projected separation, that is, the number density fraction of 1-NNS per ($\Delta\log r = 0.2$) interval. There is a marked excess of 1-NNS in the range 1−10 kAU for the multiple systems with respect to single stars.

3.2.4. Ultra-wide binary regime in Taurus?

The comparison between the pair correlation and the Ψ functions yields new insight into an extended binary regime. Both of them have the same scale-free trend at least in the four logarithm bins of separation (see Fig. 4), from 1.5 to 5 kAU. While the correlation function reaches an elbow from that point on, breaking from the binary regime to reach the clustering regime, the Ψ function extends the same power-law trend up to ~100 kAU. Thus, although it remains hidden in the correlation function because of mixing between binarity and clustering, the binary regime in Taurus appears to extend to much larger scales than previously realized.

3.3. Local neighborhood of multiples versus single stars

In this subsection, we study the spatial distribution of multiple systems and single stars based on the comparison of their 1-NNS statistics.

The S_1 sample in the whole Taurus contains 96 stars flagged as visual multiple systems (in the range of 10 AU to 1 kAU) and 242 a priori single stars. To limit biases, we define the S_3 sample composed exclusively of Class II and III stars that have been observed at HAR. From that sub-sample, we separately construct the 1-NNS histograms of the 89 multiple systems and the 140 single stars (see Fig. 5) that appear very different one from each other. Both the KS and AD statistical tests indicate that we can reject the theory that they come from the same parent population with a confidence level of 99.8%. The 1-NNS fraction of multiple systems having a projected separation less than 10 kAU is noticeably higher than for the single stars in the same range (see Fig. 5).

The excess fraction of 1-NNS at close spacings is remarkably high: nearly 40% of the 1-NNS of all multiple systems are located within the first five bins, that is, between 1 and 10 kAU.

This is more than 2.5 times the fraction found in the same range of separations for the single stars (15%). It is also twice as high as the frequency of visual companions per decade of projected separation found in the 10−2000 AU separation range (see Duchêne & Kraus 2013, Fig. 5). Moreover, 63% of the companions of multiple systems in the five first bins are themselves multiple systems (25% of the total multiple systems), against 43% for the singles (6% of total single stars sample).

The local neighborhood of multiple stars is thus more populated than that of simple stars: a multiple system has almost three times more chance of having a companion within 10 kAU, and that companion in turn has a higher chance of being a close multiple system itself than a single star.

3.4. Beyond local neighborhood

To test whether this striking difference between the neighborhood of multiple systems and single stars extends beyond the first neighbor, we analyse the second nearest neighbor distributions, again using the bias-free S_3 sample. Although there is still a slight excess of companions for multiple systems within the first bin up to 10 kAU, this difference does not appear statistically significant: the KS and AD tests both give a p-value of 0.15. We further compare their respective k-NNS distributions, up to $k = 8$. They too cannot be statistically distinguished (p-value of 1 for both KS and AD tests). This confirms the statistical identity between the neighborhood of the two populations, multiples and singles, beyond their first neighbor.

Since the 2-NNS distribution is not statistically different for single stars and multiple systems, we can use its median value (0.13°, 0.3 pc or ∼60 kAU) as a typical length scale at which these two populations cannot be statistically distinguished. This value is close to the upper clustering threshold $r_c = 0.24$ pc derived in the second section.

Interestingly, we also note that the distribution of the second nearest neighbor of multiple systems cannot be statistically distinguished from the first nearest neighbor of single stars either (p-value of 0.1224 for the KS test). This suggests that, although the neighborhood of multiple systems has been found to be more populated within 10 kAU, this trend fades away beyond 60 kAU. Based on the k-nearest neighbor analysis ($k \geq 2$), we therefore define a scale of 60 kAU beyond which the stellar environment is statistically identical for single stars and multiple systems.

4. From multiples to ultra-wide pairs

In this section, we further analyze the reasons for such a divergence between neighborhoods of multiple systems and single stars.

4.1. Mutual nearest neighbors as ultra-wide pairs

From the list of all nearest neighbor pairings (see Table C.2), we selected the subset of all mutual nearest neighbors, that is, pairs in which the nearest neighbors are reciprocal. This property serves to probe the most "connected" pairs. It has been used, for instance, as part of the process to identify physical binary candidates in simulations (Parker et al. 2009; Kouwenhoven et al. 2010).

We find that over the 338 first nearest neighbor pairings of stars in Taurus, 45% of pairings are non-mutual pairs (within this type of couples, only one star is the nearest neighbor of the other, while the second one has a different nearest neighbor) whereas 55% of the whole pairings are mutual pairs.

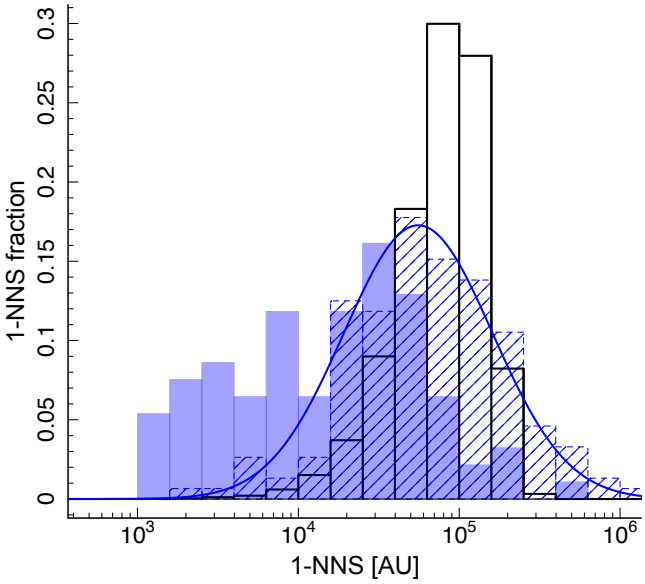

Fig. 6. Distribution of ultra-wide pair fraction as a function of separation in the three main Taurus filaments (i.e., for stars enclosed within W_{in}, solid blue histogram) versus pair fraction of random mutual pairs (obtained from 10 000 Monte Carlo samplings, thick black histogram) and 1-NNS fraction of non-mutual pairs (dashed blue histogram). The solid blue line represent a log-normal fit to the distribution of non-mutual pairs in Taurus. The distribution of mutual pairs of Taurus does not result from a random process (p-value of 10^{-16}), and is statistically different from non-mutual pairs distribution in Taurus (p-value of 10^{-14}). Conversely, the 1-NNS distribution of non-mutual pairs in Taurus is reasonably well fitted (p-value of 0.2) by a long-normal function, with a mean value $\mu = 4.74 \pm 0.04$ and a standard deviation $\sigma = 0.46 \pm 0.03$.

The 1-NNS distribution for mutual pairs is markedly different from that of non-mutual pairs; the KS test returns a p-value of 10^{-14} when assuming, as a null hypothesis, that these two populations are drawn from a same parent population (see Fig. 6). The distribution for non-mutual pairs is reasonably well fitted by a log-normal function (p-value = 0.2, showing that two distributions are statistically the same) with a mean $\mu = 4.74 \pm 0.04$ (i.e. 55 kAU) and a standard deviation $\sigma = 0.46 \pm 0.03$ (∼20 to 160 kAU range). This suggests that, unlike the mutual pairs, the distribution of 1-NNS for non-mutual pairs in Taurus may be seen as a statistical realization of a multiplicative process, which is converted to an additive process in the log domain, for which the central limit theorem may be applied. Although it is beyond the scope of this paper to establish the physical origin of this multiplicative process, we can speculate that relative random motion and gravitational encounters between physically unrelated stars may contribute to randomization of the spatial location of individual stars. This is not the case for gravitational binaries or common proper motion pairs, however, as they are kept together at the same mutual nearest distance over time.

The mutual pairs in Taurus are very unlikely due to random mutual pairing (see Fig. 6). A KS test comparing the distribution of 1-NNS separation of mutual pairs with the W_{in} window to that of the mutual first nearest pairs from an ensemble of random Monte Carlo Poisson samplings within the same window returns a p-value lower than 10^{-16}.

Moreover, it is worth noting that the mutual pairs we identified in the separation range 1–5 kAU, are already known to be true physical binaries, that is, gravitationally bound binaries

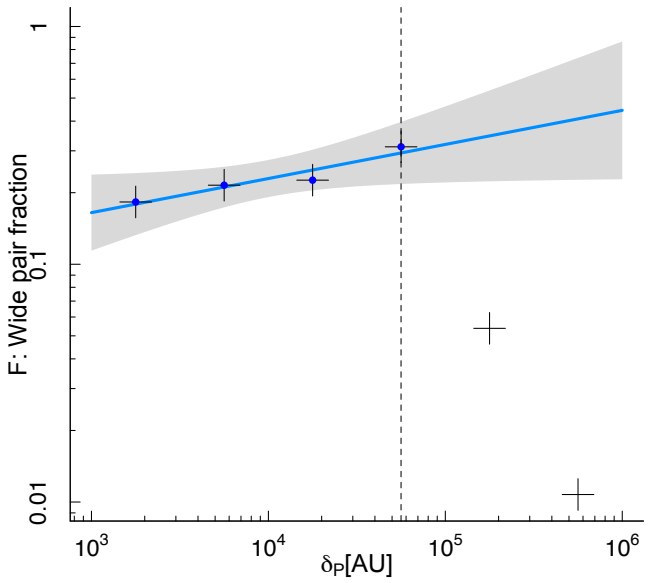

Fig. 7. Ultra-wide pair fraction F within the whole Taurus region (sample S_1) as a function of separation, plotted using $\Delta\delta_P = 0.25$ dex bins. The solid blue line is a power law fit to the data ($F = \alpha\,\delta_P^{\beta}$, with $\log\alpha = -1.21$ and $\beta = 0.14$) between 3 and ~60 kAU (vertical black dashed line). The gray area represents the 95% confidence band. In terms of the power law parameters, the corresponding parameter 95% confidence intervals are $\log\alpha = [-1.78, -0.65]$, $\beta = [0, 0.28]$.

(Kraus & Hillenbrand 2009b). This further validates our selection of mutual nearest neighbors to identify physically related pairs in that range. We thus expect that a large majority of these mutual pairs to be at least common proper-motion pairs, and plausibly even gravitationally bound. From now on, we refer to these systems as ultra-wide pairs (UWPs).

The present-day distribution of separations for these UWPs should reflect its counterpart at birth, provided that dynamical encounters are rare enough to keep it unchanged (see discussion Sect. 5). These mutual pairs covering separations from 1 to ~60 kAU are the only type of pairs (versus non-mutual pairs) found in the short-separation end of the 1-NNS distribution. Approximately 60% (resp. 90%) of 1-NNS have separations below 20 kAU (resp. 60 kAU) with a relatively long-uniform distribution. Thus, the continuous power-law trend at small and intermediate scales observed in the Ψ function is mainly due to the existence of these mutual pairs, which define the binary regime. They generate a scale-free clustering pattern and constitute a major structural spatial imprint in Taurus.

4.2. An Öpik law for the UWPs separation

In this subsection we discuss the distribution of UWP separation based on the data that we derived (see Table C.2).

The UWPs fraction F in Taurus follows a slightly increasing power law, $F \propto \delta_P^{0.14}$ (see Fig. 7), at least up to an upper cut-off of ~60 kAU (i.e., 0.27 pc). The robustness of this simple fit is confirmed by performing a power law fit to the empirical cumulative function that explains 97.73% of observed variations. Beyond this cut-off, there is a sharp decrease in the two last bins of separations. The first two bins overlap the study conducted by Kraus & Hillenbrand (2009b), who found that the separation of binaries below 4.2 kAU is log-uniform in this range ($F(\log\delta) =$ const. or, equivalently $F_O(\delta) \propto \frac{1}{\delta}$), i.e., following Opik's law.

Table 3. Class fraction in Taurus.

	Class I	Class II	Class III	N
All Taurus stars	0.11	0.52	0.37	338
Stars in UWPs ($\delta \leq 10$ kAU)	0.18	0.61	0.22	74
Stars in UWPs (all separations)	0.13	0.56	0.31	186

Notes. N is the total number of stars in each subsample.

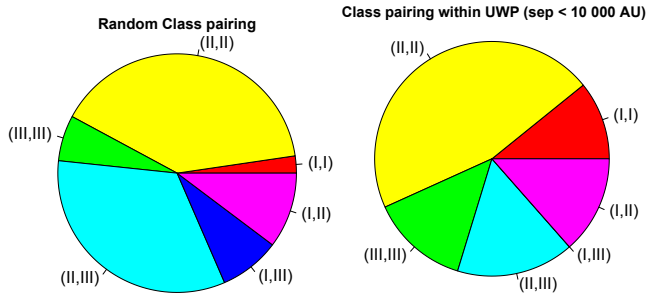

Fig. 8. Distributions of SED Class pairings expected from a random pairing process based on the global proportions of Class I, II, and III stars in Taurus (*left*) and observed among Taurus UWPs (*right*). The SED Class pairing within UWPs deviates significantly from random pairing, suggesting coevality within these systems.

4.3. Class pairing in UWPs

We first focus on the 37 mutual pairs with separation less than 10 kAU (from sample S_1), a regime where the distinction between multiple systems and single stars strongly suggests that a physical process is at play. Within this sub-population, Class I and Class II are over-represented (and, accordingly, Class III under-represented) relative to the overall Taurus population (see Table 3). A chi-squared test confirms that this difference is statistically significant (p-value of 0.01). In other words, the stellar population within UWPs separated by less than 10 kAU is less evolved, i.e., younger, than the rest of the population in the Taurus molecular cloud.

In the following, we show that the class pairing found in these UWPs deviates from random pairing. The probability P_{ij} of getting an unordered pair (i, j) without replacement is given by:

$$P_{ij} = \gamma \cdot P_i \cdot P_j = \gamma \cdot (N_i/N) \cdot \left(N'_j/(N-1)\right), \tag{11}$$

where N is the the total number of stars in the sample under consideration, $\{i, j\}$ = I, II, III is the SED Class of stars, P_i is the fraction of Class i type star, N_i is the number of stars of Class i, and $\gamma = 1$ and $N'_j = N_i - 1$ for $i = j$ whereas $\gamma = 2$ and $N'_j = N_j$ for $(i \neq j)$.

We compute the random Class pairing probability for each type of pairings from Eq. (11) and the number of stars of each Class N_i derived from the first line in Table 3. These probabilities are quite different from those observed among UWPs in Taurus (see Table 4 and Fig. 8). The main difference can be summarized as follows: there are more pairs of the same Class, that is, (I, I), (II, II) and (III, III) pairs, than expected from random pairing. Correspondingly, there are fewer pairs from mixed Classes, (I, II) and (II, III) pairs, and there are no (I, III) pairs at all despite the expectation that there should be ~10% of such pairs based on random pairing. These differences are found to be statistically significant at the 99.74% level based on a chi-squared test.

Applied to the larger sample of UWPs covering the whole range of separation (sample $P3$), we obtain the same result as

Table 4. Class pairings fraction in UWPs compared to random Class pairing.

WP type		$p_{(\mathrm{I,I})}$	$p_{(\mathrm{II,II})}$	$p_{(\mathrm{III,III})}$	$p_{(\mathrm{II,III})}$	$p_{(\mathrm{I,III})}$	$p_{(\mathrm{I,II})}$
$\delta_\mathrm{P} < 10$ kAU	UWPs	.11	.46	.14	.16	.00	.14
	Rand	.02	.36	.06	.30	.08	.18

Notes. $p_{(\mathrm{I,I})}$ is either the fraction of Class I stars paired with another Class I star within UWPs (separation δ_P less than 10 kAU) or the probability to obtain this pairing from a random distribution (*Rand*).

above with an even higher significance level ($p = 10^{-4}$). These results indicate that the UWPs are most likely coeval.

4.4. High multiplicity fraction within UWPs

Considering that the stars are part of UWPs, there are almost equal numbers of single stars (50) and multiple systems (44). The resulting multiplicity fraction of 47% is ∼15% higher than that of the sample of Class II and III stars observed at HAR that are not in UWPs, a result that is statistically significant (p-value of 0.007 for a chi-squared test). In other words, multiple systems are more often within UWPs than not. More interestingly, the multiplicity fraction within UWPs depends on the separation range: it declines from a maximum of ∼70% at short separations (at approximately 5 kAU) to the average multiplicity fraction of 47% at large separation of approximately 6 × 10 kAU, above which the multiplicity fraction remains constant (see Fig. 9). Thus, with a confidence level higher than 95%, the multiplicity fraction within UWPs is higher when their separation is shorter.

4.5. Multiplicity pairing within UWPs

In this subsection, we look at the multiplicity nature (single or multiple) of individual components composing the UWPs. There are 47 UWPs in sample S_3 with 12 of them being composed of two multiple systems (MM pairs), 15 of them of two single stars (SS pairs) and the remaining 20 pairs of one multiple system and one single star (SM pairs). The probabilities associated to random multiplicity pairings are computed from Eq. (11) and give 0.28, 0.22, and 0.50 to get a SS, SM or MM pair, respectively. Using a Pearson's χ^2 test, we cannot rule out a random multiplicity pairing (p-value 0.59) of the observed UWPs over the whole range of separation. But, the observed probability is not uniform along with the separation. For instance, considering only UWPs whose separation is less than 10 kAU, more than double the expected MM pairs are observed (48% of the UWPs are of MM pair type, 19% of SS and 33% of SM). The same χ^2 test indicates that a random multiplicity pairing can be rejected with a high significance level (p-value 0.018). Thus the higher multiplicity fraction for tighter UWPs, as shown in the previous subsection, stems primarily from the fact that multiple systems tend to be paired with other multiple systems in that range of separation (≤10 kAU).

A comparison of the pair fraction distribution between MM, SM, and SS UWPs as a function of their separation reveals indeed that nearly 90% of MM pairs are concentrated below 10 kAU, the SM pairs are distributed essentially log-uniformly over the whole range, and SS pairs are preferentially separated far apart (median separation at 35 kAU, see Fig. 10). As a consequence, MM systems are the main contributor to the observed "bump" in the 1-NNS distribution of multiple systems outlined in the previous section. Of the 30 multiple stellar

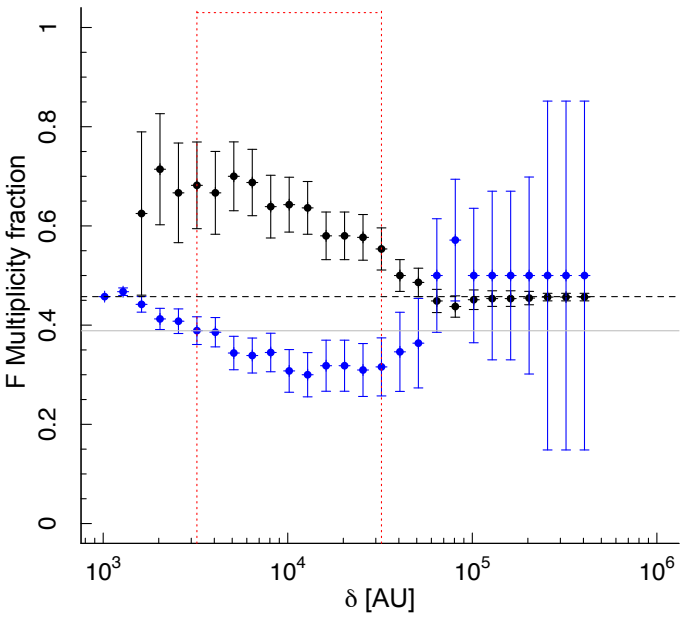

Fig. 9. Multiplicity fraction of Class II and III stars observed at HAR and members of UWPs as a function of their separation. For a given value of δ, the black (resp. blue) symbol represents the multiplicity fraction computed over all separations smaller (resp. greater) than δ. Errorbars are standard errors computed from the standard formula: $SE_i = \sqrt{F_i * (1 - F_i)/n_i} \cdot \sqrt{(N - n_i)/(N - 1)}$ where n_i is the sample size, and N is the total population size of Class II and III stars observed at HAR within UWPs independently of their separation. The dashed black line represents the mean multiplicity fraction for stars within UWPs whereas the gray line marks the corresponding mean multiplicity fraction for stars that are not in UWPs. The red dotted lines define the interval within which the multiplicity fraction within UWPs is significantly (p-value of 0.05 or less based on a chi-squared test) higher than the mean value.

systems having their 1-NNS less than 10 kAU, 20 of them are within multiple/multiple UWP (65%), 7 members (25%) are within single/multiple UWPs and 3 (10%) are non-mutual pairs. Therefore, the spatial neighborhood difference between multiple systems versus single stars comes down to a higher fraction of "tighter" MM UWPs with respect to the SS UWPs.

4.6. UWP multiplicity

In this subsection, we study the properties of UWPs, as a function of their multiplicity n_*, defined as the sum of the total number of stars within each pair ($2 \leq n_* \leq 5$).

For this analysis, we continue focusing on sample S_3 (half the population of UWPs), which has the most reliable multiplicity data, since each of the components has been observed at HAR. Within it, we investigate the distribution of the UWPs as a function of their degree of multiplicity. The number of UWPs seems to be rather uniform up to a multiplicity of four (see Table 5), and exhibits a sharp decrease for a multiplicity of five. We note that this behavior differs from the geometric progression for pre-main sequence closer binaries in Taurus $N_{n_*} \propto b^{-n_*} = 2.6^{-n_*}$ (Duchêne & Kraus 2013).

Following Correia et al. (2006), we define the multiplicity fraction per ultra-wide binary (MF_uw) as the number of higher multiplicity systems over the total number of UWP systems of the sample with projected component separations typically

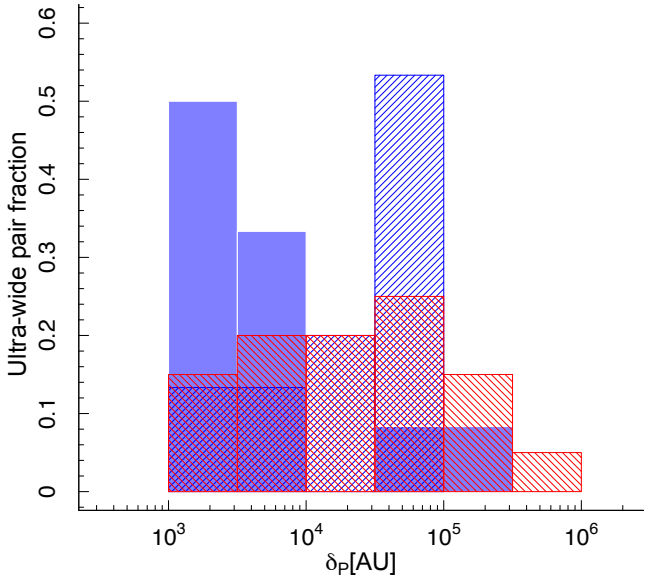

Fig. 10. SS (dashed blue), SM (dashed red) and MM (solid blue) pair fraction as a function of their separation. MM pairs are tighter (most are found below 10 kAU) whereas SS pairs are far apart (with a peak at approximately 50 kAU); on the other hand, SM pairs are relatively uniformly distributed.

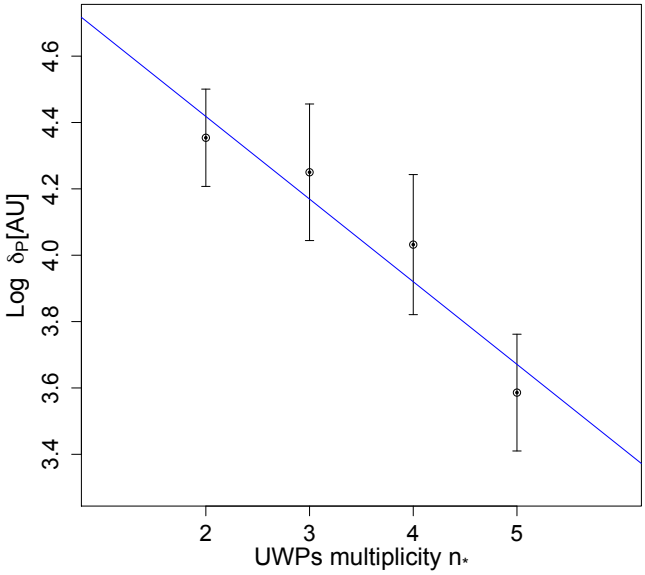

Fig. 11. Mean separation $\overline{\delta_P}$ of UWPs (sample S_3) and standard errorbars ($\pm\sigma/\sqrt{n_*}$) as a function of their multiplicity $n_* = 2, 3, ...$ The separation is consistent with a geometric progression $\delta_P \propto a^{-n_*}$ with $a \sim 1.8$ (shown as the blue line).

Table 5. Number and type of high order multiplicity in UWPs.

n_*	2	3	4	5
N_P	16	14	13	4
UWP Type	(S, S)	(S, B)	8 (B, B) 5 (S, T)	4 (B, T)
$N_{P_{60}}$	13	11	10	4
UWP Type	(S, S)	(S, B)	6 (B, B) 4 (S, T)	4 (B, T)
$N_{P_{10}}$	4	6	7	4
UWP Type	(S, S)	(S, B)	6 (B, B) 1 (S, T)	4 (B, T)

Notes. Number N_P (resp. $N_{P_{60}}$ and $N_{P_{10}}$) of UWPs in the whole range of separation (resp. for separation less than 60 kAU and 10 kAU) as a function of their multiplicity n_* and their hierarchical type (S, B, T: single, binary, triple).

higher than 1 kAU. Over the whole range of separation we obtain:

$$MF_{uw} = \frac{T + Q + \ldots}{B + T + Q + \ldots} = 65.6 \pm 11.85\%. \quad (12)$$

We similarly define the companion frequency per ultra-wide binary (CF_{uw}) as:

$$CF_{uw} = \frac{2 \times T + 3 \times Q + \ldots}{B + T + Q + \ldots} = 1.77 \pm 0.19. \quad (13)$$

We use the Poisson error to estimate the error made on MF_{uw} (resp. CF_{uw}), that is, we use the square root of the number of higher order multiple systems (resp. the total number of companions in higher order systems $2 \times T + 3 \times Q + \ldots$) divided by the total number of systems (B, T, ...). We also estimate the multiplicity fraction and companion frequency per ultra-wide binary for UWPs separated by less than 60 kAU (resp. 10 kAU): $MF_{60} = 65.79 \pm 13.16\%$ and $CF_{60} = 1.79 \pm 0.22$ (resp. $MF_{10} = 80.95 \pm 19.63\%$ and $CF_{10} = 2.33 \pm 0.33$).

The values we obtained are far above the values of multiplicity fraction ($26.8 \pm 8.1\%$) and companion frequency (0.68 ± 0.13) per wide binary found in young T Tauri wide binaries in the range 14–17 AU up to 1.7–2.3 kAU (Correia et al. 2006), highlighting the ubiquity of high-order ultra-wide binaries in Taurus found in our sample.

Based on the previous subsection, and since tighter pairs are mostly composed by MM pairs, we expect them to have a higher multiplicity. Indeed, the mean projected separation δ_P of UWPs is negatively correlated with the degree of multiplicity (see Fig. 11). We obtain the best geometric progression fit as:

$$\overline{\delta_P(n_*)} \propto a^{-n_*} \sim 1.8^{-n_*}, \quad (14)$$

where $\overline{\delta_P(N_*)}$ is the mean separation of UWPs per bin of degree of multiplicity n_*. Thus, UWPs composed of two single stars are wider on average than UWPs composed of a single star and a binary, which in turn are wider on average than UWPs composed of two multiple systems. In summary, tighter UWPs are biased towards higher-order multiplicity.

4.7. Ultra-wide pairs and mass function

The mass function of single stars and primaries of multiple systems within UWPs depends on their type (see right Fig. 12). A KS test indicates that the mass distribution for SM pairs cannot be distinguished from that of either the SS or the MM pairs. However, a similar KS test shows that the difference in mass distribution between SS and MM pairs is significant with a confidence level of 97.8%.

Specifically, compared to SS pairs, MM pairs exhibit:

- a deficit of mass below 0.1 $M_\odot$, with a frequency of only 5% (against 20%);
- a deficit of stars with mass in the 0.1–0.6 $M_\odot$ range, with a frequency of 25% for the MM pairs (against 50%);
- an excess of stars with mass between 0.6 and 0.8 $M_\odot$, with a frequency of 45% (against 25%);

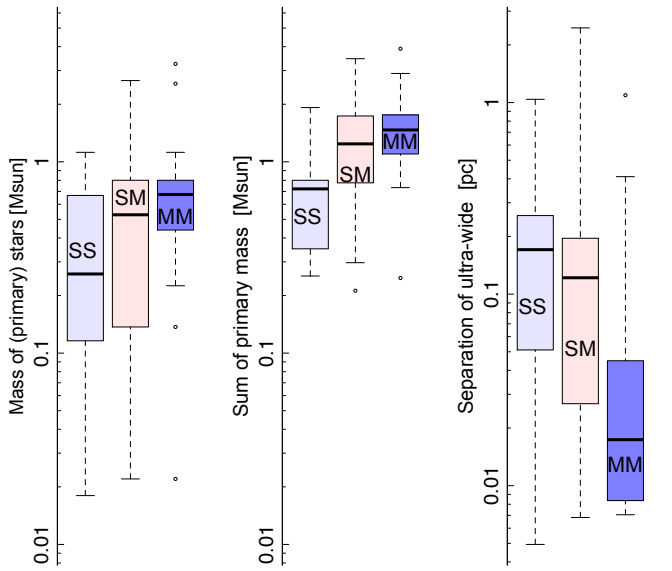

Fig. 12. Boxplot for the distribution of the (primary) star mass within UWP (*left*), the sum of the masses of the two (primary) stars within each UWP (*center*), and the separation (*right*) of UWPs. The SS, SM and MM types of systems are shown separately to illustrate that MM pairs are tighter and more massive than SS pairs.

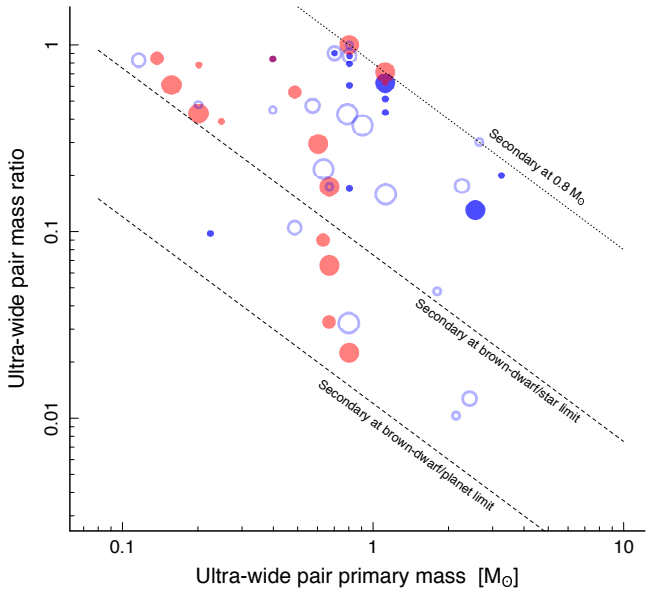

Fig. 13. Primary mass versus mass ratio within MM (filled dark blue circle), SS (filled light red circle), and SM (open light blue circle) UWPs. Intermediate (resp. smallest) size of marks: UWPs separated by less than 35 kAU (resp. less than 10 kA), the largest size devoted to wider UWPs beyond 35 kAU. Dashed lines: brown dwarfs (BD)/planet (0.012 $M_\odot$) and BD/star (0.075 $M_\odot$) limits. Dotted line: 0.8 $M_\odot$ star limit. The superpositions are due to the discretized nature of mass determination models from the spectral type and evolutionary tracks.

– a predominance of stars more massive than 0.8 $M_\odot$ (20% of the most massive stars in Taurus are in MM pairs but only 5% are in SS pairs).

Thus, 70% of stars within SS pairs have a mass of less than 0.6 $M_\odot$ and ~65% of stars within MM pairs are more massive than 0.6 $M_\odot$.

As a result of these trends (see Fig. 12), the median primary mass of MM pairs is twice as high as the median primary mass in SS pairs (0.7 $M_\odot$ compared to 0.3 $M_\odot$). Furthermore, they have a much smaller dispersion as indicated by the interquartile range for MM pairs (0.5–0.8 $M_\odot$ versus 0.1–0.7 $M_\odot$ for SS pairs, see left panel in Fig. 12). The median primary mass of MM pairs is intriguingly close to the unusual peak at 0.8 $M_\odot$ in Taurus reported by Briceño et al. (2002). This peak was tentatively explained by a fragmentation/ejection hydrodynamical model (Goodwin et al. 2004) of molecular cores that have unusual properties (extended envelope, a narrow range of core mass function with a peak near 5 $M_\odot$, and a low level of turbulence). The results of simulations show that 50% of the low-mass objects that form within the cores are ejected from their cradles to produce an extended population of low-mass stars and brown-dwarfs, whereas the remaining stars in multiple systems accrete the gas reach a mass of up to 0.8–1 $M_\odot$. This type of dynamical ejection model was also advocated by Reipurth & Clarke (2001), Boss (2001), Bate et al. (2003), Kroupa & Bouvier (2003a), Kroupa et al. (2003). However, Briceño et al. (2002) and Luhman (2006) argued that the absence of a widely dispersed brown-dwarf population is strong enough evidence to reject this type of model. Therefore up to now, there is no clear consensus to explain the peak at 0.8 $M_\odot$ in the mass function of Taurus.

Summing the two (primary) masses within each UWP amplifies the contrast between the lower mass threshold needed to produce MM pairs with respect to SS pairs (see the middle panel in Fig. 12). The median sum of primary masses within MM pairs (1.5 $M_\odot$) is twice as high as that within SS pairs (0.7 $M_\odot$), but the width of the interquartile ranges are comparable (1.2–1.7 $M_\odot$ and 0.4–0.8 $M_\odot$ for MM and SS pairs, respectively). The difference in mass range between SS and MM pairs would be even more pronounced if the mass of inner companions within MM pairs were also included in the sum; unfortunately, the current multiplicity data are insufficient to evaluate this in a consistent manner across the entire sample. In summary, the median of the stellar mass in MM pairs is twice as high as that within SS pairs, and they are also ten times less divergent; the masses of stars within SS pairs spread a larger range unlike the primary masses in MM pairs. The SM pairs have intermediate properties between these two classes.

4.8. Mass ratio in UWPs

The study of the mass ratio of the secondary mass over the primary mass in the UWPs as a function of the primary mass shows several interesting features (see Fig. 13). First the secondary mass covers the whole range of mass, from equal mass down to brown dwarf type mass (0.075 $M_\odot$) suggesting the same continuous formation scenario from star to brown dwarf. Secondly, there is a clumping trend of MM UWPs towards the upper part of the diagram. Further, we note that there are no UWPs composed of two brown dwarfs.

Some other features appear to be spurious. The apparent concentration of secondary brown dwarfs pairing with 0.6–0.8 $M_\odot$ stars showing up in Fig. 13 is in fact due to the preeminence of these 0.6–0.8 $M_\odot$ stars in the mass function. By performing 10 000 Monte Carlo mass pairing samplings amongst the mass sample of UWP stars, we obtain indeed a p-value of 0.15 compatible with the hypothesis that this pattern is due to chance pairing. The next intriguing pattern that appears at first glance is the empty top right "wedge", where no secondary stars heavier than 0.8 $M_\odot$ lie in for primary stars heavier than 0.8 $M_\odot$. By performing a similar Monte Carlo sampling, we obtain a p-value of

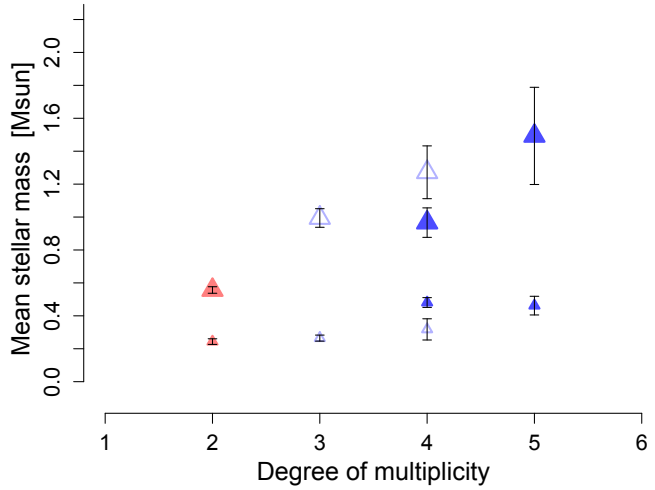

Fig. 14. Correlation between multiplicity and primary (large size mark) & secondary (small size mark) mass of stars in MM (filled dark blue triangle), SS (filled light red triangle), and SM (light blue open triangle) UWPs.

0.005, which seems to indicate that we can apparently reject the hypothesis that this occurs by chance. This result, however, is not based on a large sample size (median expectation: four pairs within that wedge), and the stellar mass determination from theoretical evolutionary tracks, as well as the spectral type classification, artificially stretches the width of this empty wedge. At this stage, we cannot therefore ensure that it is a reliable pattern.

The increase of the multiplicity goes along with the primary mass of the UWPs (see Fig. 14). This trend was also noted for closer binaries (Kraus & Hillenbrand 2007). The mass of the secondary star does not correlate with the multiplicity to the same extent.

5. Discussion

In this section, we discuss the possible nature of the UWPs identified in Taurus.

5.1. UWPs as physical pairs

The findings surrounding UWPs obtained in the previous section amount to an array of circumstantial evidence suggesting that these pairs are probably physical pairs:

- non-random 1-NNS distribution of mutual pairs (versus log-normal 1-NNS distribution for non-mutual pairs);
- approximate log-uniform separation distribution (Öpik's law distribution) for mutual pairs, extending up to ~60 kAU (i.e., 0.27 pc) at least, observed for binaries at closer separations (Kraus & Hillenbrand 2009b);
- non-random Class pairings within mutual pairs suggesting coevality;
- UWPs in the range of separation <5 kAU are already known to be true physical binaries (Kraus & Hillenbrand 2009b).

To be gravitationally bound, the internal energy of UWPs must be negative, that is, $1/2\mu\Delta v^2 - GM_1M_2/r < 0$, with μ being the reduced mass ($\mu = M_1 M_2/(M_1 + M_2)$, M_1 and M_2 being the mass of the stars), G the gravitational constant, r and Δv the separation and the relative velocity between the two stars, respectively. Thus, the condition to meet for a pair to be bound can be rewritten as follows:

$$\Delta v < (2G(M_1 + M_2)/r)^{1/2} < 0.3\left(\left[\frac{M_1}{0.5\,M_\odot}\right] + \left[\frac{M_2}{0.5\,M_\odot}\right]\right)\left(\frac{r}{10\ \mathrm{kAU}}\right)^{-1/2}\ \mathrm{km\,s^{-1}}. \quad (15)$$

This relative velocity between the stars is low compared to the observed already low velocity dispersion in the Taurus stellar complex; 2–4 $\mathrm{km\,s^{-1}}$ in the whole region (Frink et al. 1997; Rivera et al. 2015) and as low as 1–2 $\mathrm{km\,s^{-1}}$ in stellar subgroups (Jones & Herbig 1979). However, as we will see in the following subsection, the low stellar density of Taurus and the low stellar velocity dispersion prevent efficient exchanges of energy during random encounters between wide pairs and other stars, such that the characteristic disruption time τ_d of a few $\sim 10^3$ Myr is much longer than the age of the Taurus pre-main sequence population, that is, 1–10 Myr old (Kenyon & Hartmann 1995; Bertout et al. 2007; Andrews et al. 2013). Therefore, we consider in the following that UWPs are physically linked. This hypothesis will be further tested by results of the *Gaia* survey that will provide 3D spatial data and 2D/3D velocity measurements (proper motions of stars and radial velocity for part of them).

5.2. A short review on wide binaries: models and observations

From the theoretical side, different models and numerical simulations have been performed to produce multiple systems (see Reipurth et al. 2014, for a complete review on recent numerical simulation improvements). One notable result from simulations of star formation from collapsing gas is that they do not generate wide pairs at birth beyond 1 kAU because of the strong dynamical interactions that occur in simulations of the collapse of turbulent cores (Bate 2012).

Nonetheless, wide pairs are present among field stars, albeit in relatively small numbers: approximately 10% of all solar-type field stars have a companion with separations larger than 1 kAU (Raghavan et al. 2010; Lépine & Bongiorno 2007; Longhitano & Binggeli 2010) and maximum separations as high as 20 kAU (Chanamé & Gould 2004; Shaya & Olling 2011; Dhital et al. 2015).

The low-but-not-negligible fraction of visual wide pairs in the field could not solely be the result of random gravitational capture: the binary creation rate in the field is estimated to be of the order 4×10^{-21} $\mathrm{pc^{-3}\,Gyr^{-1}}$ (Kouwenhoven et al. 2010) showing that random creation of bound pairs in the field, as well as in the star-forming regions, is an extremely rare event.

An alternate mechanism must be at play to produce such pairs either at birth or as the result of subsequent dynamical evolution. But wide pairs with separations beyond 0.1 pc appear to be particularly unlikely pristine products of star formation process because their separations exceed the typical size of a collapsing cloud core, precluding a scenario based exclusively on core fragmentation.

Consequently, two scenarios based on dynamical evolution have been proposed to explain their origin. One possibility is that an initially compact triple system could dynamically unfold, with the tighter pair shrinking while the third component being ejected onto an extremely long orbit (Reipurth & Mikkola 2012). Alternatively, the gradual dissolution of a star cluster could leave behind wide binaries that are barely bound if two stars happen to be very close in the 6D phase space (Kouwenhoven et al. 2010; Moeckel & Bate 2010; Moeckel & Clarke 2011). For most star clusters, the dissolution

time, when this "pairing" could occur, is of the order of a few Gyr (Lamers & Gieles 2006).

The model of Kouwenhoven et al. (2010) also predicts that these wide pairs are high-order multiples as a reflection of the high multiplicity of individual stars at birth. This matches nicely with our findings on UWPs in Taurus, however their mechanism also induces random pairing with respect to mass and Class because the binding pairs are generated by chance depending on the proximity of the objects once the gas of the cluster is removed. This is not what is observed within UWPs in Taurus, since we have shown in the previous section that the Class-pairing is not random and that the distributions of mass is not the same in SS and MM pairs.

Another inadequacy of both the "pairing during cluster dissolution" theory and the "unfolding of triple systems" theory is that they occur on timescales that are orders of magnitude longer than the age of the Taurus population (0.1–0.5 Myr for Class I stars and a few Myr for Class II and III stars).

The large fraction of UWPs in Taurus is reminiscent of the surprisingly large number of UWPs (10–50 kAU) recently identified in slightly older moving groups (10–100 Myr) such as in the β Pic moving group (Alonso-Floriano et al. 2015). A preference has also been identified for high-order multiplicity among these UWPs, as well as in AB Doradus, TW Hydrae and Tucanae-Horologium moving groups (Torres et al. 2006; Elliott et al. 2016). Elliott & Bayo (2016) suggest that the binary population from close (0.1 AU) to very wide systems (100 kAU) in β Pic Moving Group can be accounted for by the internal dynamical interaction of triple systems as proposed by Reipurth & Mikkola (2012). But, as an alternative, these very wide pairs may be the survival part of the wide pairs population formed at an earlier time.

Some of these wide pairs may even survive longer since solar-type stars within high-order multiplicity UWPs with periods that peak around 100 yr (separations about 36.5 kAU) have also been observed in the field (Tokovinin 2014) as well as for late-spectral-type M1–M5 dwarf UWPs (Law et al. 2010). In the latter case, a very high value was found for the multiple fraction per ultra-wide pair, that is, 77^{+9}_{-22}% for systems with separations >4 kAU, very close to what we obtain for the high-order-multiple fraction derived in Taurus UWPs with separation less than 10 kAU.

On the other hand very wide pairs composed of extremely young (~0.1 Myr) Class 0 objects are relatively common (Looney et al. 2000; Tobin et al. 2010, 2016; van Kempen et al. 2012; Chen et al. 2013; Lee et al. 2015; Pineda et al. 2015). We thus conclude that the UWPs in Taurus must have been produced by a mechanism that acts extremely early on and, indeed, that these systems may well be the pristine outcome of star formation itself, as is suggested moreover by the coevality trend.

We contend that the population of UWPs that we identified in Taurus supports the idea that very wide binary systems are almost universally produced in star-forming regions, even though the physical mechanism leading to their formation remains under debate.

5.3. A pristine origin for these UWPs

To argue for pristine UWPs, one must ensure that they can survive dynamical interactions. The destruction of multiple stars occurs either due to the intrinsic instability of the non-hierarchical multiple stellar system itself or due to the decay of a few Nbody systems driven by hard or soft encounters with other stars of that region. For the former mechanism, the timescale is very short, that is, a few crossing times, or approximately a few 10 kyr (Reipurth 2000), far less than the Taurus age (few Myr).

Disruption and dissolution of wide binary stars in the Galaxy by gravitational encounters with other stars, molecular clouds, and tidal forces due to gravitational potential of the Galaxy is a long-standing study (Chandrasekhar 1944; Heggie 1975, 1977; Retterer & King 1982; Bahcall et al. 1985; Jiang & Tremaine 2010). It was estimated that in the solar neighborhood, the half-life of a binary composed of two solar-type stars separated by 31 kAU is 10 Gyr (Jiang & Tremaine 2010).

We expect that in a low-stellar-density region such as Taurus (i.e., 1–10 pc^{-2}), dynamical interactions between stellar systems are rare and soft. We thus expect minor dynamical destruction of the wide pairs in Taurus, such that most probably wide binaries in Taurus reveal their pristine configuration. The following arguments on characteristic times associated with the destruction of binaries due to dynamical encounters will give some support to these expectations.

Binney & Tremaine (2008) have estimated the effects of dynamical encounters of binaries with random stars, allowing us to derive two destruction timescales for wide binaries. First, we consider catastrophic single encounters, characterized by a timescale

$$\tau_{\rm D} = \sqrt{3/14}\,\pi^{-1}\,M_{\rm tot}^{1/2}\,(G^{1/2}\,\rho_{\rm c}\,M_{\rm c}\,a^{3/2})^{-1};$$
$$\tau_{\rm D} \sim 7.2\,{\rm Gyr}\left(\frac{M_{\rm tot}}{2\,M_\odot}\right)^{1/2}\frac{0.05\,{\rm pc}^{-3}}{\rho_{\rm c}}\frac{1\,M_\odot}{M_{\rm c}}\left(\frac{10^4\,{\rm AU}}{a}\right)^{3/2}. \quad (16)$$

Secondly, we evaluate the destruction timescale in the diffusive regime:

$$\tau_{\rm d} \sim 0.085\,(\sigma_{\rm rel}M_{\rm tot}b_{\rm min}^2)(GM_{\rm c}^2\rho_{\rm c}a^3)^{-1};$$
$$\tau_{\rm d} \sim 3.5\,{\rm Gyr}\frac{k_{\rm diff}}{0.085}\frac{\sigma_{\rm rel}}{4\,{\rm km\,s^{-1}}}\frac{M_{\rm tot}}{2\,M_\odot}\left(\frac{1\,M_\odot}{M_{\rm c}}\right)^2\frac{0.05\,{\rm pc}^{-3}}{\rho_{\rm c}}\frac{10^4\,{\rm AU}}{a}. \quad (17)$$

In both cases, a is the semimajor axis, $M_{\rm tot}$ is the total mass of the pair, $\rho_{\rm c}$ is the stellar volumic density, $M_{\rm c}$ is the mass of the random encounter star, $\sigma_{\rm rel}$ is the stellar dispersion velocity, and $k_{\rm diff} = 0.085(b_{\rm min}/a)^2$ is a diffusive parameter with $b_{\rm min} \sim a$ being the impact parameter cut off.

While the semi-major axis a cannot be estimated directly for these long period binaries, it is statistically correlated with the projected separation δ, as $\delta \approx a$ (Leinert et al. 1993; Tokovinin & Lépine 2012). The closeness of the two values depends on the chosen eccentricity distribution type, either flat ($f(e)$ = const.), as observed in solar-type stars from the Hipparcos catalog by Raghavan et al. (2010) for wide binaries, or thermalized ($f(e) = 2e$), as first theoretically proposed by Jeans (1919), generalized to broader types of distribution by Ambartsumian (1937) and observed in field stars by Duquennoy & Mayor (1991).

We evaluate the volume density through $\rho_{\rm c} = \rho_{\rm w}/\Delta \sim 1/25 \sim 0.04\,{\rm pc}^{-3}$, with $\rho_{\rm w}$ being the mean projected surface density (Eq. (1)) and $\Delta \sim 20$ pc the depth of Taurus (Torres et al. 2007).

Both destruction times are much larger than the age of the young Taurus star-forming region. Therefore, in such an environment, it is extremely unlikely that wide binaries, even with separation as large as 100 kAU, can be destroyed by dynamical encounters. Numerical simulations have indeed confirmed that loose associations such as Taurus provide an environment that is inefficient at binary disruption even at large separation

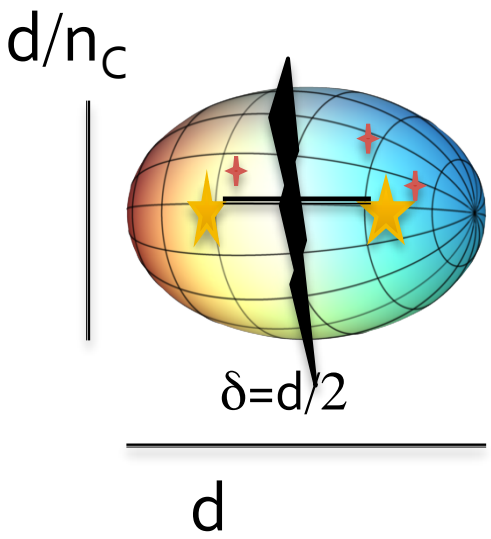

Fig. 15. Schematics for a prolate core with a length d in the main direction and a width of d/n_c giving birth to two multiple systems whose primaries are separated by δ.

(Kroupa & Bouvier 2003b; Marks & Kroupa 2012). Even if they use an initial distribution of binary separation up to 10 kAU, we expect that a same result would be obtained with an extended binary separation up to 100 kAU.

We may thus feel confident that the very wide pairs populations in Taurus may trace the initial spatial distribution at birth without being destroyed by dynamical encounters up to now.

5.4. Core properties for pristine UWPs

In the context of a pristine configuration for the wide pairs, we look for the initial conditions that could lead to the formation of such pairs in a core fragmentation model (see Fig. 15).

We thus make the hypotheses that; (1) these UWPs are pristine remnants of the star-formation process; and (2) they form within a single core with a core-to-star efficiency factor $\alpha_C \sim 40\%$ (Könyves et al. 2015). The total mass of parental clump can be evaluated as $M_{\rm tot}(1+\alpha_{\rm B})/\alpha_{\rm C}$, where $M_{\rm tot}$ is the sum of (primary) masses and $\alpha_{\rm B}\, M_{\rm tot}$ is the mass of inner companion stars ($\alpha_{\rm B} = 0$ for SS pairs). We also introduce a geometrical shape factor $n_{\rm c}$ to quantify the propension of clumps to be elongated and prolate rather than roundish or oblate ($n_{\rm c} \sim 2$–4, Myers et al. 1991; Ryden 1996; Lomax et al. 2013). From those assumptions, we get the mean particle density ρ of an initial core as:

$$\rho = M_{\rm tot}/(\mu\, m_{\rm H}) \left(4/3\,\pi\, n_C^2 \delta^3\right)^{-1} (1+\alpha_{\rm B})/\alpha_C, \tag{18}$$

where $\mu = 2.33$ is the mean molecular weight and $m_{\rm H}$ is the atomic hydrogen mass.

We proceed to compute the median density estimate of initial cores that would be required to produce each type of pair $\rho_{\rm SS}, \rho_{\rm SM}, \rho_{\rm MM}$:

$$\rho_{\rm SS} \sim 10^4\ {\rm cm}^{-3} \left[\frac{M_{\rm tot}}{0.72\,M_\odot}\right]\left[\frac{0.17\,{\rm pc}}{\delta}\right]^3 \frac{[n_C/4]^2}{[\alpha_C/0.5]}, \tag{19a}$$

$$\rho_{\rm SM} \sim 10^5\ {\rm cm}^{-3} \left[\frac{M_{\rm tot}}{1.24\,M_\odot}\right]\left[\frac{0.12\,{\rm pc}}{\delta}\right]^3 \frac{[n_C/4]^2\,(1+[\alpha_B/0.2])}{[\alpha_C/0.5]}, \tag{19b}$$

$$\rho_{\rm MM} \sim 3\times 10^7\ {\rm cm}^{-3} \left[\frac{M_{\rm tot}}{1.47\,M_\odot}\right]\left[\frac{0.017\,{\rm pc}}{\delta}\right]^3 \frac{[n_C/4]^2\,(1+[\alpha_B/0.2]}{[\alpha_C/0.5]}. \tag{19c}$$

We then question whether those kinds of cores would be instable or stable against any perturbation. As the Jeans instability length is given by:

$$\lambda = c_{\rm s}\left(\frac{\pi}{G\rho}\right)^{1/2}, \tag{20}$$

where $c_{\rm s} = 0.2\ {\rm km\,s}^{-1}$ is the sound speed at $T = 10$ K, we derive the following Jeans length estimates for the three types of pairs:

$$\lambda_{\rm SS} = 1.2\left[\frac{\delta_{\rm SS}}{0.17}\right]{\rm pc}, \tag{21a}$$

$$\lambda_{\rm SM} = 0.7\left[\frac{\delta_{\rm SM}}{0.12}\right]{\rm pc}, \tag{21b}$$

$$\lambda_{\rm MM} = 0.2\left[\frac{\delta_{\rm MM}}{0.017}\right]{\rm pc}, \tag{21c}$$

where $\delta_{\rm SS}, \delta_{\rm SM}, \delta_{\rm MM}$ are the median separations of the three types of UWPs.

The Jeans length is therefore slightly larger than the characteristic length of the SS fictitious clumps (Eq. (21a)), while it is smaller for the MM and SM ones (Eqs. (21b) and (21c)). In other words, the latter two appear to be instable against gravitational (Jeans) instability, while the former appears to be marginally stable.

Therefore, it is plausible that SM and MM pairs formed within the same core, while the SS pairs may have formed through an alternative scenario. We may still consider a pristine origin for them. The two stars may be born in two distinct but proximate cores. Or alternatively, the two stars may be born within the same low-density core that becomes supercritical due to the external potential of the Galaxy (Ballesteros-Paredes et al. 2009b,a) or due to the tidal potential of the parent molecular cloud (Horton et al. 2001), both scenarios triggering enhanced fragmentation.

5.5. Towards a fragmentation cascade scenario

We note a negative correlation between the multiplicity within the UWPs and their separation (see Fig. 11): the multiplicity decreases with wider separation. The fragmentation of dense molecular cores into UWPs with at least one high-mass ($\gtrsim 0.5\,M_\odot$) component seems to have an impact on the probability that either one component, and most probably both, will further fragment. The extent of this fragmentation cascade would depend on the separation of the first two fragments. It suggest a competitive scenario between collapse and an efficient fragmentation process of the gas core/clump to create multiple systems rather than one single object. The densest and most massive molecular cores in Taurus would produce high multiplicity hierarchical MM UWPs. Based on the work of Kraus et al. (2011), this fragmentation cascade scenario may be inhibited at lower spatial scales, since they found that there is no relation between a 1–5 kAU-wide binary and innermost high-order multiplicity distribution.

The probable primordial nature of UWPs suggests a scenario in which the turbulent fragmentation of a molecular filament forms over-densities (Pineda et al. 2015) that undergo a fragmentation cascade, producing wide pairs that are themselves closer multiple systems. These systems may be stable enough to

survive 1–30 Myr in a low-density environment. This link between multiple systems and wide pairs has also been outlined by millimeter observations that show that fragmentation of clumps can proceed through separate envelopes or inside a common envelope (Looney et al. 2000).

5.6. Distributed and clustered modes of formation clues in Taurus

Taurus is considered as the archetypical star-forming region that gives rise to isolated prestellar cores, with a typical density of 10^5 cm^{-3} and a size of 0.1 pc. The consensus model for star formation therefore predicts that this cloud will produce a distributed star population, in contrast with the clustered star-formation mode that is associated with denser regions such as ρ Ophiuchus, with typical core densities of 10^7 cm^{-3} and sizes of 0.02–0.03 pc (Ward-Thompson et al. 2007). In this context, it is worth noting the significant (more than two orders of magnitude) difference between the typical densities derived for the hypothesized cores that give birth to the SM pairs and MM pairs. These results suggest that, despite its overall low core densities, the Taurus molecular cloud may harbor the two modes of star formation, isolated and clustered.

6. Conclusion

In the Taurus star-forming complex, we have identified an extended binary regime up to ∼60 kAU using the one point correlation function, Ψ, which further allowed us to distinguish three spatial regimes. The clustering regime has an upper clustering threshold of 0.1° (0.24 pc, i.e., 50 kAU, at the distance of Taurus). The Ψ function appears to be scale-free ($\psi = r^{-1.53}$) over three decades and extends the usual binary regime, as defined by the two-point correlation function, to a very wide pair regime. We note that the value of the upper clustering length coincides with the local maximum of Taurus NH^{2+} molecular cores correlation function reported by Hacar et al. (2013). As the latter indicates a typical separation between the cores, we expect to see a clustering imprint of stars starting at this value, as is observed. This length is more than twice the universal typical width (0.1 pc) of filamentary structures highlighted by *Herschel* in Taurus and more generally in Gould Belt star-forming regions (André et al. 2014). The clustering regime is followed by a regime of stellar inhibition between 0.1° and 0.5° (0.24 pc up to 1.2 pc), and ends beyond this with a third regime associated to highly isolated stars.

We have highlighted a major structural pattern in the spatial distribution of stars in Taurus based on their multiplicity status. Distinguishing single stars from multiple systems, defined as having at least one physical companion within 1 kAU, we highlight a major and unexpected difference in their spatial distribution based on 1-NNS study: the stellar neighborhood in the range of 1−10 kAU of multiple stars is more "crowded" than the single star neighborhood: 40% of multiple systems have a companion within that range compared to 15% for single stars. The probability that a multiple system has a wide companion is threefold that of a single star. We have shown that this excess within 10 kAU is due to the very wide pairs candidates that are moreover generally composed themselves of two multiple systems.

We have identified a potential very wide pairs population in Taurus. Our work shows that 55% of our stellar catalog in Taurus are UWPs in the range of 1−60 kAU. These UWPs are composed preferentially of stars of the same Class, departing from random Class pairing, and, thus, pointing towards coeval pairs. The pair fraction of UWPs follows an almost flat Öpik function ($r^{0.14}$), extending what has been found for the young binaries at lower range. This coevality clue and Öpik law behavior coupled with the fact that their 1-NNS distribution differs from random mutual pairs suggests that these may be true physical pairs; indeed, UWPs with separation less than 5 kAU have been found to be wide binaries (Kraus & Hillenbrand 2009b).

Amongst the UWP population in Taurus, we distinguish three different types of UWPs, depending on whether they are composed either of two multiple systems (MM pairs), a single star and a multiple system (SM pairs), or two single stars (SS pairs). Their properties differ in terms of (primary) mass and separation range. The MM pairs are composed of more massive stars (median mass: 0.65 $M_\odot$) and tighter (median value 3.5 kAU, 75% of them having separation below 9 kAU). The median mass of stars within SS pairs is 0.25 $M_\odot$ and their median separation is 35 kAU (75% of them have a separation above 12 kAU). SM pairs have intermediate properties (median mass of primaries of 0.5 $M_\odot$ and a uniform separation distribution covering the whole range 1−60 kAU). Multiplicity in these UWPs is a decreasing function of stellar primary mass. We also show that the multiplicity within UWPs increases as the separation of (primary) stars decreases, showing an increased high-order-multiple fraction for the tightest UWP targets in Taurus. Class

These differences suggest a different scenario for the formation of UWPs in Taurus. The "massive" MM pairs most probably reflect the imprints of the star-formation process within the same molecular core. Based on estimates of their hypothesized natal core properties, Taurus may generate both isolated and clustered star formation. The "low-mass" SS pairs could point to a different formation scenario or may result from a dynamical process, such as low-mass star ejection from multiple systems.

Obtaining parallaxes and proper motions for all Taurus members would help tremendously in identifying which of the UWPs are physical binaries, common proper motion pairs and those which may form from a dynamical process. This will ultimately be achieved thanks to the *Gaia* survey that will determine the astrometric quantities (angular position, proper motion, and parallax) of stars with an accuracy of 20 μ and at a brightness of 15 mag, and determine the radial velocity of stars brighter than 16 mag.

Unfortunately, the first *Gaia* release (Gaia Collaboration 2016) does not provide enough data on the whole sample of stars in Taurus (only ∼5%). We expect that future releases of *Gaia*, perhaps as early as the second release, will allow us to firmly establish the physical status of the UWPs, in turn providing a means to discriminate between different scenarios for their formation, and more generally will provide invaluable information on the structure and dynamics of Taurus as a young association (Moraux 2016).

In summary, we identified a new category of ultra-wide pairs (UWPs) in Taurus outlining a high order of multiplicity for tighter ones (separation less than 10 kAU). We suggest that part of these UWPs may be pristine imprints of their spatial configuration at birth and put forward a cascade fragmentation scenario for their formation. Furthermore, UWPs may constitute a potential link between the wide pairs recently identified in very young Class 0 type objects (≲0.5 Myr) and the somewhat older but still young moving groups (∼20–30 Myr).

Acknowledgements. The authors would like to thank Lee Mundy for helpful discussions and Marc Pound for reading the first draft of this article. We also want to sincerely thank the anonymous referee who helped us to improve both the scientific and language aspects of this paper. This work was funded by the French national research agency through ANR 2010 JCJC 0501-1 DESC (PI E. Moraux).

References

Ahn, S., & Fessler, A. 2003, Standard Errors of Mean, Variance, and Standard Deviation Estimators, Tech. Rep., Technical Report, Ann Arbor, MI, USA
Alonso-Floriano, F. J., Caballero, J. A., Cortés-Contreras, M., Solano, E., & Montes, D. 2015, A&A, 583, A85
Alves, J., Lombardi, M., & Lada, C. J. 2007, A&A, 462, L17
Ambartsumian, V. A. 1937, Astron. Zh., 14, 207
Andre, P., Ward-Thompson, D., & Barsony, M. 1993, ApJ, 406, 122
André, P., Di Francesco, J., Ward-Thompson, D., et al. 2014, Protostars and Planets VI (Tuscon: University of Arizona Press), 27
Andrews, S. M., Rosenfeld, K. A., Kraus, A. L., & Wilner, D. J. 2013, ApJ, 771, 129
Baddeley, A., & Turner, R. 2005, J. Statist. Software, 12, 1
Bahcall, J. N., Hut, P., & Tremaine, S. 1985, ApJ, 290, 15
Ballesteros-Paredes, J., Gómez, G. C., Loinard, L., Torres, R. M., & Pichardo, B. 2009a, MNRAS, 395, L81
Ballesteros-Paredes, J., Gómez, G. C., Pichardo, B., & Vázquez-Semadeni, E. 2009b, MNRAS, 393, 1563
Bate, M. R. 2012, MNRAS, 419, 3115
Bate, M. R., Bonnell, I. A., & Bromm, V. 2003, MNRAS, 339, 577
Benaglia, T., Chauveau, D., Hunter, D. R., & Young, D. 2009, J. Stat. Software, 32, 1
Bertout, C., Siess, L., & Cabrit, S. 2007, A&A, 473, L21
Binney, J., & Tremaine, S. 2008, in Galactic Dynamics, second edition (Princeton University Press)
Boss, A. P. 2001, ApJ, 551, L167
Briceño, C., Luhman, K. L., Hartmann, L., Stauffer, J. R., & Kirkpatrick, J. D. 2002, ApJ, 580, 317
Burrows, C. J., Stapelfeldt, K. R., Watson, A. M., et al. 1996, ApJ, 473, 437
Carney, M. T., Yıldız, U. A., Mottram, J. C., et al. 2016, A&A, 586, A44
Chakraborty, A., & Ge, J. 2004, AJ, 127, 2898
Chakraborty, A., Feigelson, E. D., & Babu, G. J. 2014, Astrolabe: Astronomy Users Library for R, r package version 0.1
Chanamé, J., & Gould, A. 2004, ApJ, 601, 289
Chandrasekhar, S. 1943, Rev. Mod. Phys., 15, 1
Chandrasekhar, S. 1944, ApJ, 99, 54
Chen, X., Arce, H. G., Zhang, Q., et al. 2013, ApJ, 768, 110
Connelley, M. S., Reipurth, B., & Tokunaga, A. T. 2008, AJ, 135, 2496
Connelley, M. S., Reipurth, B., & Tokunaga, A. T. 2009, AJ, 138, 1193
Correia, S., Zinnecker, H., Ratzka, T., & Sterzik, M. F. 2006, A&A, 459, 909
Covey, K. R., Greene, T. P., Doppmann, G. W., & Lada, C. J. 2006, AJ, 131, 512
Daemgen, S., Bonavita, M., Jayawardhana, R., Lafrenière, D., & Janson, M. 2015, ApJ, 799, 155
Dahl, D. B. 2014, xtable: Export tables to LaTeX or HTML, r package version 1.7-4
Dhital, S., West, A. A., Stassun, K. G., Schluns, K. J., & Massey, A. P. 2015, AJ, 150, 57
Di Folco, E., Dutrey, A., Le Bouquin, J.-B., et al. 2014, A&A, 565, L2
Dobbs, C. L., Krumholz, M. R., Ballesteros-Paredes, J., et al. 2014, Protostars and Planets VI (Tuscon: University of Arizona Press), 3
Duchêne, G. 1999, A&A, 341, 547
Duchêne, G., & Kraus, A. 2013, ARA&A, 51, 269
Duchêne, G., Ghez, A. M., McCabe, C., & Weinberger, A. J. 2003, ApJ, 592, 288
Duchêne, G., Bontemps, S., Bouvier, J., et al. 2007, A&A, 476, 229
Duquennoy, A., & Mayor, M. 1991, A&A, 248, 485
Elliott, P., & Bayo, A. 2016, MNRAS, 459, 4499
Elliott, P., Bayo, A., Melo, C. H. F., et al. 2016, A&A, 590, A13
Esplin, T. L., Luhman, K. L., & Mamajek, E. E. 2014, ApJ, 784, 126
Frink, S., Röser, S., Neuhäuser, R., & Sterzik, M. F. 1997, A&A, 325, 613
Gaia Collaboration (Brown, A. G. A., et al.) 2016, A&A, 595, A2
Ghez, A. M., Neugebauer, G., & Matthews, K. 1993, AJ, 106, 2005
Ghez, A. M., White, R. J., & Simon, M. 1997, ApJ, 490, 353
Gladwin, P. P., Kitsionas, S., Boffin, H. M. J., & Whitworth, A. P. 1999, MNRAS, 302, 305
Gomez, M., Hartmann, L., Kenyon, S. J., & Hewett, R. 1993, AJ, 105, 1927
Goodwin, S. P., Whitworth, A. P., & Ward-Thompson, D. 2004, A&A, 419, 543
Goodwin, S. P., Nutter, D., Kroupa, P., Ward-Thompson, D., & Whitworth, A. P. 2008, A&A, 477, 823
Graffelman, J. 2013, calibrate: Calibration of Scatterplot and Biplot Axes, r package version 1.7.2
Greene, T. P., Wilking, B. A., Andre, P., Young, E. T., & Lada, C. J. 1994, ApJ, 434, 614
Hacar, A., Tafalla, M., Kauffmann, J., & Kovács, A. 2013, A&A, 554, A55
Harrell, F., E., Dupont, C., & others. 2015, Hmisc: Harrell Miscellaneous, r package version 3.16-0
Harris, A. 2013, FITSio: FITS (Flexible Image Transport System) utilities, r package version 2.0-0
Hartmann, L. 2002, ApJ, 578, 914
Heggie, D. C. 1975, MNRAS, 173, 729
Heggie, D. C. 1977, Rev. Mex. Astron. Astrofis., 3, 169
Herczeg, G. J., & Hillenbrand, L. A. 2014, ApJ, 786, 97
Holman, K., Walch, S. K., Goodwin, S. P., & Whitworth, A. P. 2013, MNRAS, 432, 3534
Horton, A. J., Bate, M. R., & Bonnell, I. A. 2001, MNRAS, 321, 585
Ireland, M. J., & Kraus, A. L. 2008, ApJ, 678, L59
Itoh, Y., Hayashi, M., Tamura, M., et al. 2005, ApJ, 620, 984
Jeans, J. H. 1919, MNRAS, 79, 408
Jiang, Y.-F., & Tremaine, S. 2010, MNRAS, 401, 977
Jones, B. F., & Herbig, G. H. 1979, AJ, 84, 1872
Juvela, M., & Montillaud, J. 2016, A&A, 585, A78
Kendall, M., & Stuart, A. 1977, The advanced theory of statistics, 4th edn., Vol. 1: Distribution theory (New York, NY: Macmillan)
Kenyon, S. J., & Hartmann, L. 1995, ApJS, 101, 117
Kerscher, M., Szapudi, I., & Szalay, A. S. 2000, ApJ, 535, L13
Kirk, H., & Myers, P. C. 2011, ApJ, 727, 64
Kohler, R., & Leinert, C. 1998, A&A, 331, 977
Konopacky, Q. M., Ghez, A. M., Rice, E. L., & Duchêne, G. 2007, ApJ, 663, 394
Könyves, V., André, P., Men'shchikov, A., et al. 2015, A&A, 584, A91
Koresko, C. D. 2000, ApJ, 531, L147
Kouwenhoven, M. B. N., Goodwin, S. P., Parker, R. J., et al. 2010, MNRAS, 404, 1835
Kraus, A. L., & Hillenbrand, L. A. 2007, ApJ, 662, 413
Kraus, A. L., & Hillenbrand, L. A. 2008, ApJ, 686, L111
Kraus, A. L., & Hillenbrand, L. A. 2009a, ApJ, 704, 531
Kraus, A. L., & Hillenbrand, L. A. 2009b, ApJ, 703, 1511
Kraus, A. L., & Hillenbrand, L. A. 2012, ApJ, 757, 141
Kraus, A. L., White, R. J., & Hillenbrand, L. A. 2006, ApJ, 649, 306
Kraus, A. L., Ireland, M. J., Martinache, F., & Hillenbrand, L. A. 2011, ApJ, 731, 8
Kroupa, P., & Bouvier, J. 2003a, MNRAS, 346, 369
Kroupa, P., & Bouvier, J. 2003b, MNRAS, 346, 343
Kroupa, P., Bouvier, J., Duchêne, G., & Moraux, E. 2003, MNRAS, 346, 354
Lada, C. J. 1987, in Star Forming Regions, eds. M. Peimbert, & J. Jugaku, IAU Symp., 115, 1
Lada, C. J., & Lada, E. A. 2003, ARA&A, 41, 57
Lada, C. J., & Wilking, B. A. 1984, ApJ, 287, 610
Lada, C. J., Muench, A. A., Rathborne, J., Alves, J. F., & Lombardi, M. 2008, ApJ, 672, 410
Lamers, H. J. G. L. M., & Gieles, M. 2006, A&A, 455, L17
Landy, S. D., & Szalay, A. S. 1993, ApJ, 412, 64
Larson, R. B. 1995, MNRAS, 272, 213
Law, N. M., Dhital, S., Kraus, A., Stassun, K. G., & West, A. A. 2010, ApJ, 720, 1727
Lee, K. I., Dunham, M. M., Myers, P. C., et al. 2015, ApJ, 814, 114
Leinert, C., Zinnecker, H., Weitzel, N., et al. 1993, A&A, 278, 129
Leinert, C., Richichi, A., & Haas, M. 1997, A&A, 318, 472
Lépine, S., & Bongiorno, B. 2007, AJ, 133, 889
Lomax, O., Whitworth, A. P., & Cartwright, A. 2013, MNRAS, 436, 2680
Longhitano, M., & Binggeli, B. 2010, A&A, 509, A46
Looney, L. W., Mundy, L. G., & Welch, W. J. 2000, ApJ, 529, 477
Luhman, K. L. 2004, ApJ, 617, 1216
Luhman, K. L. 2006, ApJ, 645, 676
Luhman, K. L., Allen, P. R., Espaillat, C., Hartmann, L., & Calvet, N. 2010, ApJS, 186, 111
Luhman, K. L., Mamajek, E. E., Shukla, S. J., & Loutrel, N. P. 2017, AJ, 153, 46
Marks, M., & Kroupa, P. 2012, A&A, 543, A8
Marsh, K. A., Kirk, J. M., André, P., et al. 2016, MNRAS, 459, 342
Mathieu, R. D. 1994, ARA&A, 32, 465
Moeckel, N., & Bate, M. R. 2010, MNRAS, 404, 721
Moeckel, N., & Clarke, C. J. 2011, MNRAS, 415, 1179
Monnier, J. D., Tannirkulam, A., Tuthill, P. G., et al. 2008, ApJ, 681, L97
Moraux, E. 2016, EAS Pub. Ser., 80-81, 73
Myers, P. C., Fuller, G. A., Goodman, A. A., & Benson, P. J. 1991, ApJ, 376, 561
Nychka, D., Furrer, R., & Sain, S. 2015, R-fields: Tools for Spatial Data, r package version 8.2-1
Offner, S. S. R., Clark, P. C., Hennebelle, P., et al. 2014, Protostars and Planets VI (Tuscon: University of Arizona Press), 53
Padgett, D. L., Brandner, W., Stapelfeldt, K. R., et al. 1999, AJ, 117, 1490
Parker, R. J., Goodwin, S. P., Kroupa, P., & Kouwenhoven, M. B. N. 2009, MNRAS, 397, 1577

Peebles, P. J. E. 1980, in Ninth Texas Symposium on Relativistic Astrophysics, eds. J. Ehlers, J. J. Perry, & M. Walker, Annals of the New York Academy of Sciences, 336, 161
Pineda, J. E., Offner, S. S. R., Parker, R. J., et al. 2015, Nature, 518, 213
R Core Team 2015, R: A Language and Environment for Statistical Computing, R Foundation for Statistical Computing, Vienna, Austria
Raghavan, D., McAlister, H. A., Henry, T. J., et al. 2010, ApJS, 190, 1
Rebull, L. M., Padgett, D. L., McCabe, C.-E., et al. 2010, ApJS, 186, 259
Reipurth, B. 2000, AJ, 120, 3177
Reipurth, B., & Clarke, C. 2001, AJ, 122, 432
Reipurth, B., & Mikkola, S. 2012, Nature, 492, 221
Reipurth, B., & Zinnecker, H. 1993, A&A, 278, 81
Reipurth, B., Clarke, C. J., Boss, A. P., et al. 2014, Protostars and Planets VI (Tuscon: University of Arizona Press), 267
Retterer, J. M., & King, I. R. 1982, ApJ, 254, 214
Rivera, J. L., Loinard, L., Dzib, S. A., et al. 2015, ApJ, 807, 119
Robotham, A. 2015, magicaxis: Pretty Scientific Plotting with Minor-Tick and log Minor-Tick Support, r package version 1.9.4
Ryden, B. S. 1996, ApJ, 471, 822
Sakhr, J., & Nieminen, J. M. 2006, Phys. Rev. E, 73, 036201
Sartoretti, P., Brown, R. A., Latham, D. W., & Torres, G. 1998, A&A, 334, 592
Shaya, E. J., & Olling, R. P. 2011, ApJS, 192, 2
Shu, F. H., Adams, F. C., & Lizano, S. 1987, ARA&A, 25, 23
Simon, M. 1997, ApJ, 482, L81
Simon, M., Ghez, A. M., Leinert, C., et al. 1995, ApJ, 443, 625
Simon, M., Beck, T. L., Greene, T. P., et al. 1999, AJ, 117, 1594
Smith, K. W., Balega, Y. Y., Duschl, W. J., et al. 2005, A&A, 431, 307
Tafalla, M., & Hacar, A. 2015, A&A, 574, A104
Therneau, T. 2014, deming: Deming, Thiel-Sen and Passing-Bablock Regression, r package version 1.0-1
Tobin, J. J., Hartmann, L., Looney, L. W., & Chiang, H.-F. 2010, ApJ, 712, 1010
Tobin, J. J., Looney, L. W., Li, Z.-Y., et al. 2016, ApJ, 818, 73
Todorov, K., Luhman, K. L., & McLeod, K. K. 2010, ApJ, 714, L84
Todorov, K. O., Luhman, K. L., Konopacky, Q. M., et al. 2014, ApJ, 788, 40
Tokovinin, A. 2014, AJ, 147, 87
Tokovinin, A., & Lépine, S. 2012, AJ, 144, 102
Torres, C. A. O., Quast, G. R., da Silva, L., et al. 2006, A&A, 460, 695
Torres, R. M., Loinard, L., Mioduszewski, A. J., & Rodríguez, L. F. 2007, ApJ, 671, 1813
van Kempen, T. A., Longmore, S. N., Johnstone, D., Pillai, T., & Fuente, A. 2012, ApJ, 751, 137
Vincenty, T. 1975, Survey Review, 22, 88
Ward-Thompson, D., André, P., Crutcher, R., et al. 2007, Protostars and Planets V (Tuscon: University of Arizona Press), 33
White, R. J., & Ghez, A. M. 2001, ApJ, 556, 265
Ysard, N., Abergel, A., Ristorcelli, I., et al. 2013, A&A, 559, A133

Appendix A: Spherical geometry

As a reminder, this section gives the formulae to obtain the angular distance $\Delta\sigma$ between two stars on the celestial sphere, given by the spherical law of cosines:

$$\Delta\sigma = \arccos(\sin\alpha_1 \sin\alpha_2 + \cos\alpha_1 \cos\alpha_2 \cos\Delta\delta), \tag{A.1}$$

where ϕ_i, λ_i $(i = 1, 2)$ are, respectively, the declination and right ascension of the star i, and $\Delta\delta = |\delta_2 - \delta_1|$ their absolute difference in declination. Since this above equation is ill-conditioned for small $\Delta\sigma$, it is better to use the following Vincenty formula (Vincenty 1975) applied to a sphere

$$\Delta\sigma = \arctan\left(\frac{\sqrt{(\cos\alpha_2 \sin\Delta\delta)^2 + (\cos\alpha_1 \sin\alpha_2 - \sin\phi_1 \cos\alpha_2 \cos\Delta\delta)^2}}{\sin\alpha_1 \sin\alpha_2 + \cos\alpha_1 \cos\alpha_2 \cos\Delta\delta}\right). \tag{A.2}$$

Appendix B: Analytics for *k*-Nearest Neighborhood statistics

B.1. Theoretical probability density function (PDF) and cumulative distribution of 1-nearest neighbor separation (1-NNS) for spatial random distribution

In this section, we derive the theoretical distribution of 1-NNS for a random point process in an infinite medium, following the work done in 3D by Chandrasekhar (1943). The probability $w(r)\mathrm{d}r$ that the first neighbor of a star is located at a distance between r and $r + \mathrm{d}r$ in 2D, is given by the product of the probability that there is no stars in a disk of radius r multiplied by the probability of having stars in a shell area between r and $r + \mathrm{d}r$:

$$w(r)\mathrm{d}r = \left(1 - \int_0^r w(r)\mathrm{d}r\right) \times 2\pi r\, \mathrm{d}r\, \rho, \tag{B.1}$$

where ρ is the mean intensity of the process in an infinite medium, that is, the average number of stars per unit of surface. Equation (B.1) may be written as:

$$\frac{\mathrm{d}}{\mathrm{d}r}\left(\frac{w(r)}{2\pi r\rho}\right) = -2\pi r\rho \frac{w(r)}{2\pi r\rho}. \tag{B.2}$$

Once integrated, from the equation above, we get the probability density function (PDF) of the first neighbor distance for a random Poissonnian process:

$$w(r) = 2\pi\rho r \exp(-\pi\rho r^2). \tag{B.3}$$

The PDF integral is unity (i.e., we have $\int_0^{+\infty} w(r)\mathrm{d}r = \left[-\exp(-\pi\rho r^2)\right]_0^{+\infty} = 1$).

Furthermore, from the 1-NNS PDF (Eq. (B.3)), we get the related cumulative distribution function $W(r)$ as:

$$\begin{aligned} W(r) &= \int_0^r 2\pi\rho r \exp(-\pi\rho r^2)\mathrm{d}r \\ &= 1 - \exp(-\pi\rho r^2), \end{aligned} \tag{B.4}$$

that allows us to define the characteristic value r_q associated to the quantile q from: $q = W(r_q) = 1 - \exp(-\pi\rho r_q^2)$, to get:

$$r_q = \sqrt{\ln(1/(1-q))/(\pi\rho)}. \tag{B.5}$$

B.2. Moments of first nearest neighbor distribution

B.2.1. Mean

The theoretical mean $\bar{r}_t$ of the first nearest neighbor distance in an infinite medium is computed from the PDF as:

$$\begin{aligned} \bar{r}_t = \mathbb{E}(r) &= \int_0^{+\infty} r\, w(r)\mathrm{d}r \\ &= \left[\frac{\mathrm{erf}(\sqrt{\pi\rho}r)}{2\sqrt{\rho}} - r\exp(-\pi\rho r^2)\right]_0^{+\infty}, \end{aligned} \tag{B.6}$$

where $=\mathbb{E}(r)$ is the expected value of r, and $\mathrm{erf}(x)$ is the error function. Taking the value at 0 and infinity, we end up with a simple analytical result of first nearest neighbor distance theoretical mean $\bar{r}_t$ in a random process of intensity ρ in an infinite medium, i.e., $\bar{r}_t$ is strictly equal to half of the inverse square root of the density:

$$\bar{r}_t \simeq \frac{1}{2\sqrt{\rho}}. \tag{B.7}$$

B.2.2. Variance

From the PDF $w(r)$, we now compute the theoretical variance σ_t^2 (σ_t being the standard deviation) of the first nearest neighbor distance for a random Poisson process,

$$\begin{aligned} \sigma_t^2 &= \int_0^{+\infty} (r - \bar{r})^2 w(r)\,\mathrm{d}r \\ &= 2\pi\rho \int_0^{+\infty} r\left(r - \frac{1}{2\sqrt{\rho}}\right)^2 \exp(-\pi\rho r^2)\,\mathrm{d}r. \end{aligned} \tag{B.8}$$

The integration gives:

$$\begin{aligned} \sigma_t^2 = \frac{-1}{4\pi\rho}\Big[&\exp(-\pi\rho r^2)\left(2\pi\exp(\pi\rho\, r^2)\,\mathrm{erf}(\sqrt{\pi\rho}\, r)\right) \\ &+ \pi(1 - 2\sqrt{a}\, r)^2 + 4\Big]_0^{+\infty}. \end{aligned} \tag{B.9}$$

We then compute series expansions of the integral at $x = 0$:

$$\begin{aligned} \lim_{r\to 0}\sigma_t^2 = &-\frac{4+\pi}{4\pi\rho} + \frac{\pi r^2}{4} - \frac{2}{3}\pi\sqrt{\rho}r^3 \\ &- \frac{1}{8}(\pi - 4)\pi\rho r^4 + O(r^5), \end{aligned} \tag{B.10}$$

and then at $x = +\infty$:

$$\begin{aligned} \lim_{r\to+\infty}\sigma_t^2 = -1/(2\rho)\Big(&\exp(-\pi r^2)[2\rho r^2 - 2\sqrt{\rho} \\ &+ (1/2 + 2/\pi) - (\sqrt{\rho}\,\pi r)^{-1} \\ &+ (2\rho^{2/3}\pi^2 r3)^{-1} + O(r^{-4})] + 1\Big), \end{aligned} \tag{B.11}$$

to finally get:

$$\begin{aligned} \sigma_t^2 &= -(2\rho)^{-1} + (4+\pi)(4\pi\rho)^{-1} \\ &= (4-\pi)(4\pi\rho)^{-1}. \end{aligned} \tag{B.12}$$

B.2.3. Skewness

The skewness of a distribution quantifies its asymmetry, and is defined from the third moment of the distribution. When it is positive, the peak of the distribution is shifted to the left, that is, there is a tail towards the right. When it is negative, it is the other way round. The skewness may be defined from the moments of the distribution:

$$\begin{aligned}\gamma_t &= \left(\mathbb{E}(r^3) - 3\bar{r}_t\mathbb{E}(r^2) + 2{\bar{r}_t}^3\right)/(\sigma_t)^3\\ &= \left(3/(4\pi\rho^{3/2}) - 3\bar{r}_t/(\pi\rho) + 2{\bar{r}_t}^3\right)/(\sigma_t)^3\\ &= 2\sqrt{\pi}(\pi-3)/(4-\pi)^{3/2}\\ &\approx 0.63. \end{aligned} \tag{B.13}$$

We note that the skewness of the first nearest neighbor distribution of a random spatial distribution is constant, that is, independent of the density/intensity of the random process.

B.3. Log PDF

Based on transformation rules, we then derive the theoretical PDF for the Log(1-NNS) in a random process. Let $y = \mathrm{Log}(r)$, where r is the 1-NNS variable, and thus we have:

$$w(r)\mathrm{d}r = w(y)\mathrm{d}y, \tag{B.14}$$

where $w(r)$ is the PDF of the 1-NNS variable (Eq. (B.3)) and $w(y)$ is the PDF of the logarithm variable. We get the following moments for the random k1-NNS theoretical distributions:

$$w(y) = w(r)\left|\frac{\partial r}{\partial y}\right| = w(r)\frac{\mathrm{d}r}{\mathrm{d}y}\cdot \tag{B.15}$$

From this relation, we get the PDF of the first neighbor distance logarithm for a random process as:

$$w(y) = 2\,\ln(10)\,\pi\,\rho\,r^2\,\exp\left(-\pi\rho r^2\right), \tag{B.16}$$

where it reaches its maximun value (mode) at $r_{\mathrm{mod}} = \sqrt{\pi\rho}$. From Taylor expansion for $x \ll 1$, we get:

$$w(y) \sim 2\,\ln(10)\,\pi\,\rho\,r^2\,+O(x^4), \tag{B.17}$$

as we expect in 2D for a random distribution, the first nearest neighbor 1-NNS distribution function increases as a squared power law for $r \ll 1/\sqrt{\pi\rho}$. From Eq. (B.16) above, we derive its logarithmic expression:

$$\log w(y) = \log(2\,\ln(10)\,\pi\,\rho\,) + 2\,r\,-(\pi\rho/\ln 10\,)r^2. \tag{B.18}$$

In a Poisson point process in a d-dimensional space with intensity ρ, the distance r between a point and its kth neighbor is distributed according to the generalized Gamma distribution:

$$\mathcal{P}_k(r) \approx \tfrac{d}{r}\,\frac{[\rho V_{\mathrm{d}}(r)]^k}{\Gamma(k)}\cdot\exp\left(-\rho V_{\mathrm{d}}(r)\right). \tag{B.19}$$

where $V_{\mathrm{d}}(r)$ is the volume ball or radius r in d-space.

$$V_{\mathrm{d}}(r) = c_{\mathrm{d}}r^d, \tag{B.20}$$

and c_{d} is the unit volume ball in d-space given by:

$$c_{\mathrm{d}} = \pi^{d/2}/\Gamma(d/2+1), \tag{B.21}$$

and Γ is the Gamma function. So, in a planar (2D) distribution, we get:

$$\mathcal{P}_k(r) = \frac{2(\pi\rho)^k}{\Gamma(k)}\cdot r^{2k-1}\cdot\exp\left(-\rho\pi r^2\right). \tag{B.22}$$

The cumulative distribution is then:

$$\mathcal{W}_k(r) = \int_0^r \mathcal{P}_k(r)\mathrm{d}r. \tag{B.23}$$

So for the second nearest neighbor cumulative distribution we get:

$$\mathcal{W}_2(r) = \int_0^r \mathcal{P}_2(r)\mathrm{d}r = 1-(\pi\rho r^2+1)\,\exp(-\pi r^2), \tag{B.24}$$

and for the third nearest neighbor cumulative distribution, we have:

$$\mathcal{W}_3(r) = \int_0^r \mathcal{P}_3(r)\mathrm{d}r = 1/2\left[\exp(-\pi r^2)\left(-\pi\rho r^2(\pi\rho r^2+2)-2\right)+2\right]. \tag{B.25}$$

Appendix C: Catalogs

This section gathers the catalogs described respectively in Sects. 2 and 4.1 of the paper.

Table C.1. Taurus stars catalog.

#	2MASS	Name	RA_*J*2000	Dec_*J*2000	SpT	M [$M_\odot$]	Class	n_*	Sep [″]	HAR	HAR Ref.
1	J04034930+2610520	HBC358A+B+C	60.955	26.18	M3.5	0.335	III	4	0.15,1.58,3.15	Y	L93, D99
2	J04034997+2620382	XEST06-006	60.958	26.34	M5.25	0.157	III	1	–	N	
3	J04035084+2610531	HBC359	60.962	26.18	M2	0.575	III	1	–	N	
4	J04043936+2158186	HBC360	61.164	21.97	M3.5	0.335	III	1	–	Y	L93
5	J04043984+2158215	HBC361	61.166	21.97	M3	0.398	III	1	–	Y	L93
6	J04044307+2618563	IRAS 04016+2610	61.179	26.32	K3	1.796	I	1	–	Y	P99, C08
7	J04053087+2151106	HBC362	61.379	21.85	M2	0.575	III	1	–	N	
8	J04080782+2807280	–	62.033	28.12	M3.75	0.303	III	2	0.052	Y	K11, K12
9	J04131414+2819108	LkCa1	63.309	28.32	M4	0.271	III	1	–	N	
10	J04132722+2816247	Anon1	63.363	28.27	M0	0.701	III	2	0.0149	Y	L93, K11
11	J04135328+2811233	IRAS 04108+2803A	63.472	28.19	M4c	0.271	I	1	–	Y	C08
12	J04135471+2811328	IRAS 04108+2803B	63.478	28.19	M2c	0.575	I	1	–	N	
13	J04135737+2918193	IRAS 04108+2910	63.489	29.31	M0	0.701	II	1	–	N	
14	J04141188+2811535	–	63.550	28.20	M6.25	0.086	II	1	–	Y	K12, T14
15	–	IRAS 04111+2800G	63.551	28.14	M2c	0.575	I	1	–	N	
16	J04141291+2812124	V773TauA+B	63.554	28.20	K3	1.796	II	3	−1.,0.049,0.244	Y	L93, G93, D03, D15
17	J04141358+2812492	FMTau	63.557	28.21	M0	0.701	II	1	–	Y	L93, K11
18	J04141458+2827580	FNTau	63.561	28.47	M5	0.178	II	1	–	Y	L93, G93, K11
19	J04141700+2810578	CWTau	63.571	28.18	K3	1.796	II	1	–	Y	L93, G93, K11
20	J04141760+2806096	CIDA1	63.573	28.10	M5.5	0.137	II	1	–	Y	W16
21	J04142639+2805597	MHO2	63.610	28.10	M2.5	0.486	II	3	0.050,4.00	Y	C08, W16
22	J04143054+2805147	MHO3	63.627	28.09	K7	0.801	II	2	0.031	Y	W16
23	J04144730+2646264	FPTau	63.697	26.77	M4	0.271	II	1	–	Y	L93, K11
24	J04144739+2803055	XEST20-066	63.697	28.05	M5.25	0.157	III	1	–	N	
25	J04144786+2648110	CXTau	63.699	26.80	M2.5	0.486	II	1	–	Y	L93, K11
26	J04144797+2752346	LkCa3A+B	63.700	27.88	M1	0.633	III	2	−1.,−1.,0.491	Y	L93, G93
27	J04144928+2812305	FOTauA+B	63.705	28.21	M3.5	0.335	II	2	0.166	Y	L93, G93
28	J04145234+2805598	XEST20-071	63.718	28.10	M3.25	0.366	III	1	–	N	
29	J04150515+2808462	CIDA2	63.771	28.15	M5.5	0.137	III	2	0.053	Y	W16
30	J04151471+2800096	KPNO1	63.811	28.00	M8.5	0.022	III	1	–	Y	K06
31	J04152409+2910434	–	63.850	29.18	M7	0.057	III	1	–	Y	K12, T14
32	J04153916+2818586	–	63.913	28.32	M3.75	0.303	II	1	–	N	
33	J04154278+2909597	IRAS 04125+2902	63.928	29.17	M1.25	0.618	II	1	–	N	
34	J04155799+2746175	–	63.992	27.77	M5.5	0.137	II	1	–	N	
35	J04161210+2756385	–	64.050	27.94	M4.75	0.201	II	1	–	Y	K07
36	J04161885+2752155	–	64.079	27.87	M6.25	0.086	III	1	–	Y	K12, T14

Notes. This catalog was built from Luhman et al. (2010) and Kirk & Myers (2011). All the multiple systems with a separation less than 1 kAU is set to be one entry (see Sect. 2). The following sources are listed in Luhman et al. (2010) but not included here: HBC351, HBC352, HBC353, HBC355(+354), HBC356, V410TauAnon20, LH0422+15, CIDA13. Columns 1–3: star reference number (this work), 2MASS Point Source Catalog and common Name. Column 4–5: ecliptic right ascension and Declination (Epoch J2000). Columns 6–8: spectral type, (Primary) mass, Class. Columns 9–15: total number of stars (n_*) within 1000 AU (spectroscopic binaries not counted as membership), Separation of companions stars with the primary, Flag (Y/N) to mention wether the stellar system/star has been observed at High Angular Resolution and reference papers associated to each star/stellar system.

References. B96: Burrows et al. (1996); C04: Chakraborty & Ge (2004); C08: Connelley et al. (2008); C09: Connelley et al. (2009); C06: Correia et al. (2006); D15: Daemgen et al. (2015); D99: Duchêne (1999); D03: Duchêne et al. (2003); D07: Duchêne et al. (2007); D16: Duchêne et al. (in prep.); F14: Di Folco et al. (2014); G93: Ghez et al. (1993); G97: Ghez et al. (1997); I05: Itoh et al. (2005); I08: Ireland & Kraus (2008); K98: Kohler & Leinert (1998); K07: Konopacky et al. (2007); K00: Koresko (2000); K06: Kraus et al. (2006); K11: Kraus et al. (2011); K12: Kraus & Hillenbrand (2012); L93: Leinert et al. (1993); L97: Leinert et al. (1997); M08: Monnier et al. (2008); P99: Padgett et al. (1999); R93: Reipurth & Zinnecker (1993); S98: Sartoretti et al. (1998); S95: Simon et al. (1995); S99: Simon et al. (1999); S05: Smith et al. (2005); T10: Todorov et al. (2010); T14: Todorov et al. (2014); W01: White & Ghez (2001); W16: White et al. (in prep.).

Table C.1. continued.

#	2MASS	Name	RA_J2000	Dec_J2000	SpT	M [$M_\odot$]	Class	n_*	Sep [$''$]	HAR	HAR Ref.
37	J04162725+2053091	–	64.114	20.89	M5	0.178	III	1	–	Y	K12
38	J04162810+2807358	LkCa4	64.117	28.13	K7	0.801	III	1	–	Y	L93, K11
39	J04163048+3037053	–	64.127	30.62	M4.5	0.225	III	1	–	N	
40	J04163911+2858491	–	64.163	28.98	M5.5	0.137	II	1	–	Y	K12
41	J04173372+2820468	CYTau	64.391	28.35	M1.5	0.604	II	1	–	Y	L93, G93, K11
42	J04173893+2833005	LkCa5	64.412	28.55	M2	0.575	III	2	0.048	Y	L93, S98, K11
43	J04174955+2813318	KPNO10	64.456	28.23	M5	0.178	II	1	–	Y	K12
44	J04174965+2829362	V410X-ray1	64.457	28.49	M4	0.271	II	1	–	Y	K11, W16
45	J04180796+2826036	V410X-ray3	64.533	28.43	M6	0.096	III	2	0.049	Y	K06, K12, W16
46	J04181078+2519574	V409Tau	64.545	25.33	M1.5	0.604	II	1	–	N	
47	J04181710+2828419	V410Anon13	64.571	28.48	M5.75	0.116	II	1	–	Y	K06, W16
48	J04182147+1658470	HBC372	64.589	16.98	K5	1.121	III	1	–	Y	S98
49	J04182909+2826191	V410Anon25	64.621	28.44	M1	0.633	III	1	–	N	
50	J04183030+2743208	KPNO11	64.626	27.72	M5.5	0.137	III	1	–	N	
51	J04183110+2827162	V410TauA+B+C	64.630	28.45	K7	0.801	III	3	0.123,0.287	Y	L93, G93, G97
52	J04183112+2816290	DDTauA+B	64.630	28.27	M3.5	0.335	II	2	0.56	Y	L93, G93
53	J04183158+2816585	CZTauA+B	64.632	28.28	M3	0.398	II	2	0.33	Y	L93
54	J04183203+2831153	IRAS 04154+2823	64.633	28.52	M2.5	0.486	I	1	–	N	
55	J04183444+2830302	V410X-ray2	64.644	28.51	M0	0.701	II	1	–	N	
56	J04184023+2824245	V410X-ray4	64.668	28.41	M4	0.271	III	1	–	N	
57	J04184061+2819155	V892Tau	64.669	28.32	B9	3.250	II	3	0.060,4.10	Y	L97, S05, M08
58	J04184133+2827250	LR1	64.672	28.46	K4.5	1.378	II	1	–	N	
59	J04184250+2818498	V410X-ray7	64.677	28.31	M0.75	0.650	II	2	0.032	Y	W16
60	J04184703+2820073	Hubble4	64.696	28.34	K7	0.801	III	2	−1.,0.0284	Y	L93, G93, K11
61	J04185115+2814332	KPNO2	64.713	28.24	M7.5	0.044	III	1	–	Y	K06
62	J04185147+2820264	CoKuTau/1	64.715	28.34	M0	0.701	II	2	0.25	Y	P99, W16
63	J04185170+1723165	HBC376	64.715	17.39	K7	0.801	III	1	–	Y	L93, K11
64	J04185813+2812234	IRAS 04158+2805	64.742	28.21	M5.25	0.157	I	1	–	N	
65	J04190110+2819420	V410X-ray6	64.755	28.33	M5.5	0.137	II	1	–	N	
66	J04190126+2802487	KPNO12	64.755	28.05	M9	0.013	II	1	–	Y	K06
67	J04190197+2822332	V410X-ray5a	64.758	28.38	M5.5	0.137	III	1	–	Y	W16
68	J04191281+2829330	FQTauA+B	64.803	28.49	M3	0.398	II	2	0.79	Y	L93
69	J04191583+2906269	BPTau	64.816	29.11	K7	0.801	II	1	–	Y	L93, G93, K11
70	J04192625+2826142	V819Tau	64.859	28.44	K7	0.801	II	1	–	Y	L93, G93, K11
71	J04193545+2827218	FRTau	64.898	28.46	M5.25	0.157	II	1	–	N	
72	J04194127+2749484	LkCa7A+B	64.922	27.83	M0	0.701	III	2	1.05	Y	L93
73	J04194148+2716070	IRAS 04166+2708	64.923	27.27	M0c	0.701	I	1	–	N	
74	–	IRAS 04166+2706	64.927	27.23	M3c	0.398	I	1	–	N	
75	J04194657+2712552	[GKH94]41	64.944	27.22	M7.5	0.044	I	1	–	N	
76	J04195844+2709570	IRAS 04169+2702	64.994	27.17	M0c	0.701	I	2	0.18	Y	C08
77	J04201611+2821325	–	65.067	28.36	M6.5	0.076	II	1	–	Y	T14
78	J04202144+2813491	–	65.089	28.23	M1	0.633	II	1	–	Y	D16
79	J04202555+2700355	–	65.106	27.01	M5.25	0.157	II	1	–	Y	K12
80	J04202583+2819237	IRAS 04173+2812	65.108	28.32	M3c	0.398	II	1	–	N	
81	J04202606+2804089	–	65.109	28.07	M3.5	0.335	II	1	–	N	
82	J04203918+2717317	XEST16-045	65.163	27.29	M4.5	0.225	III	1	–	N	
83	J04205273+1746415	J2-157	65.220	17.78	M5.5	0.137	III	1	–	Y	W16
84	J04210795+2702204	–	65.283	27.04	M5.25	0.157	II	1	–	Y	K07
85	J04210934+2750368	–	65.289	27.84	M5.25	0.157	II	1	–	N	
86	J04211038+2701372	IRAS 04181+2654B	65.293	27.03	K7	0.801	I	1	–	Y	C08
87	J04211146+2701094	IRAS 04181+2654A	65.298	27.02	M3	0.398	I	1	–	Y	C08
88	J04213459+2701388	–	65.394	27.03	M5.5	0.137	II	1	–	Y	K07, K12
89	J04214013+2814224	XEST21-026	65.417	28.24	M5.75	0.116	III	1	–	N	
90	J04214323+1934133	IRAS 04187+1927	65.430	19.57	M0	0.701	II	1	–	Y	W16
91	J04214631+2659296	–	65.443	26.99	M5.75	0.116	II	1	–	Y	K12

Table C.1. continued.

#	2MASS	Name	RA_J2000	Dec_J2000	SpT	M [$M_\odot$]	Class	n_*	Sep [″]	HAR	HAR Ref.
92	J04215450+2652315	–	65.477	26.88	M8.5	0.022	III	1	–	Y	K12, T14
93	J04215563+2755060	DETau	65.482	27.92	M1	0.633	II	1	–	Y	L93, G93, K11
94	–	IRAM 04191+1522	65.487	15.50	M5c	0.178	0	1	–	N	
95	J04215740+2826355	RYTau	65.489	28.44	K1	2.265	II	1	−1	Y	L93, G93, K11
96	J04215884+2818066	HD 283572	65.495	28.30	G5	2.616	III	1	–	Y	L93, G93, S95, K11
97	J04215943+1932063	TTauN+S	65.498	19.54	K0	2.430	II	3	0.053,0.71	Y	L93, G93, K00
98	J04220043+1530212	IRAS 04191+1523A	65.502	15.51	M3c	0.398	I	2	5.97	Y	C08
99	J04220069+2657324	Haro6-5B	65.503	26.96	K5	1.121	I	1	–	Y	P99, C08
100	J04220217+2657304	FSTauA+B	65.509	26.96	M0	0.701	II	2	0.264	Y	L93, S95, C08, C09
101	J04220313+2825389	LkCa21	65.513	28.43	M3	0.398	III	2	0.0444	Y	L93, K11
102	J04221332+1934392	–	65.555	19.58	M8	0.031	III	1	0.051	Y	T14
103	J04221568+2657060	XEST11-078	65.565	26.95	M1	0.633	I	1	–	N	
104	J04221644+2549118	–	65.568	25.82	M7.75	0.038	III	1	–	Y	K12, T14
105	J04221675+2654570	–	65.570	26.92	M1.5	0.604	II	1	–	Y	K07
106	J04222404+2646258	XEST11-087	65.600	26.77	M4.75	0.201	III	1	–	N	
107	J04224786+2645530	IRAS 04196+2638	65.699	26.76	M1	0.633	II	1	–	N	
108	J04230607+2801194	–	65.775	28.02	M6	0.096	II	1	–	Y	K12
109	J04230776+2805573	IRAS 04200+2759	65.782	28.10	M5c	0.178	II	1	–	N	
110	J04231822+2641156	–	65.826	26.69	M3.5	0.335	II	1	–	N	
111	J04233539+2503026	FUTauA	65.897	25.05	M7.25	0.051	II	2	5.7	N	
112	J04233919+2456141	FTTau	65.913	24.94	M1c	0.633	II	1	–	Y	L93, K11
113	J04242090+2630511	–	66.087	26.51	M6.5	0.076	II	1	–	Y	T14
114	J04242646+2649503	–	66.110	26.83	M5.75	0.116	II	1	–	Y	K12
115	J04244457+2610141	IRAS 04216+2603	66.186	26.17	M0.5	0.667	II	1	–	N	
116	J04244506+2701447	J1-4423	66.188	27.03	M5	0.178	III	1	–	N	
117	J04245708+2711565	IPTau	66.238	27.20	M0	0.701	II	1	–	Y	L93, K11
118	J04251767+2617504	J1-4872A	66.324	26.30	K7	0.801	III	4	0.051,0.174,3.32	Y	D99, C06, W16
119	J04262939+2624137	KPNO3	66.622	26.40	M6	0.096	II	1	–	Y	K06
120	J04263055+2443558	–	66.627	24.73	M8.75	0.018	II	1	–	Y	T14
121	J04265352+2606543	FVTauA+B	66.723	26.12	K5	1.121	II	2	0.69	Y	L93, G93, S95, D15
122	J04265440+2606510	FVTau/cA+B	66.727	26.11	M2.5	0.486	II	2	0.743	Y	L93, S95
123	J04265629+2443353	IRAS 04239+2436	66.735	24.73	M2c	0.575	I	2	0.3	Y	D07, C08
124	J04265732+2606284	KPNO13	66.739	26.11	M5	0.178	II	1	–	Y	W16
125	J04270266+2605304	DGTauB	66.761	26.09	K2c	2.134	I	1	–	Y	P99
126	J04270280+2542223	DFTauA+B	66.762	25.71	M2	0.575	II	2	0.088	Y	L93, G93, S95
127	J04270469+2606163	DGTau	66.770	26.10	K6	0.906	II	1	–	Y	L93, G93, S95, C08, C09, K11
128	J04270739+2215037	–	66.781	22.25	M6.75	0.067	III	1	–	Y	K12, T14
129	J04272799+2612052	KPNO4	66.867	26.20	M9.5	0.013	III	1	–	Y	K06
130	J04274538+2357243	–	66.939	23.96	M8.25	0.026	III	1	–	Y	T14
131	J04275730+2619183	IRAS 04248+2612	66.989	26.32	M4.5	0.225	I	3	0.160,4.55	Y	P99, C08
132	-	L1521F-IRS	67.162	26.86	M7c	0.057	I	1	–	N	
133	J04284263+2714039	–	67.178	27.23	M5.25	0.157	II	2	0.627	Y	K07, K12
134	J04290068+2755033	–	67.253	27.92	M8.25	0.026	II	1	–	Y	K12, T14
135	J04290498+2649073	IRAS 04260+2642	67.271	26.82	K5.5	1.013	II	1	–	N	
136	J04292071+2633406	J1-507	67.336	26.56	M4	0.271	III	2	0.0794	Y	K11, W16
137	J04292165+2701259	IRAS 04263+2654	67.340	27.02	M5.25	0.157	II	2	1.29	Y	K07
138	J04292373+2433002	GVTauA+B	67.349	24.55	K5	1.121	I	2	1.29	Y	D07
139	J04292971+2616532	FWTauA+B+C	67.374	26.28	M5.5	0.137	III	3	0.160/2.23	Y	S95, W01, K14
140	J04293008+2439550	IRAS 04264+2433	67.375	24.67	M1	0.633	I	1	–	N	
141	J04293209+2430597	–	67.384	24.52	M3c	0.398	I	1	–	N	
142	J04293606+2435556	XEST13-010	67.400	24.60	M3	0.398	III	1	–	N	
143	J04294155+2632582	DHTauA+B	67.423	26.55	M1	0.633	II	2	2.34	Y	L93, S95, I05, K11, K14
144	J04294247+2632493	DITauA+B	67.427	26.55	M0	0.701	III	2	0.12	Y	L93, G93, S95, K11
145	J04294568+2630468	KPNO5	67.440	26.51	M7.5	0.044	III	1	–	Y	K06

Table C.1. continued.

#	2MASS	Name	RA_J2000	Dec_J2000	SpT	M [$M_\odot$]	Class	n_*	Sep [″]	HAR	HAR Ref.
146	J04295156+2606448	IQTau	67.465	26.11	M0.5	0.667	II	1	–	Y	L93, G93, S95, K11
147	J04295422+1754041	–	67.476	17.90	M4	0.271	III	1	–	N	
148	J04295950+2433078	–	67.498	24.55	M5	0.178	II	1	–	Y	K07, K12
149	J04300399+1813493	UXTauA+C	67.517	18.23	K5	1.121	II	4	0.138,2.7,5.9	Y	L93, D99, K11
150	J04300724+2608207	KPNO6	67.530	26.14	M8.5	0.022	II	1	–	Y	K06
151	J04302365+2359129	–	67.599	23.99	M8.25	0.026	III	1	–	Y	K12, T14
152	J04302961+2426450	FXTauA+B	67.623	24.45	M1	0.633	II	2	0.9	Y	L93, G93, S95
153	J04304425+2601244	DKTauA	67.684	26.02	K7	0.801	II	2	2.53	Y	L93, G93, S95, K11
154	J04305028+2300088	IRAS 04278+2253A+B	67.710	23.00	G8	2.562	I	1	–	N	
155	J04305137+2442222	ZZTau	67.714	24.71	M3	0.398	II	2	0.029	Y	L93, S95
156	J04305171+2441475	ZZTauIRS	67.715	24.70	M5	0.178	II	1	–	Y	W16
157	J04305718+2556394	KPNO7	67.738	25.94	M8.25	0.026	II	1	–	Y	K06
158	J04311444+2710179	JH56	67.810	27.17	M0.5	0.667	II	1	–	Y	K11, W16
159	J04311578+1820072	MHO9	67.816	18.34	M4.25	0.248	III	1	–	Y	W16
160	J04311907+2335047	–	67.829	23.58	M7.75	0.038	III	1	–	Y	K12, T14
161	J04312382+2410529	V927TauA+B	67.849	24.18	M4.75	0.201	III	2	0.3	Y	K12, T14
162	J04312405+1800215	MHO4	67.850	18.01	M7	0.057	III	1	–	Y	K98, K06, W16
163	J04312669+2703188	–	67.861	27.06	M7.5	0.044	III	1	–	Y	K12, T14
164	J04313407+1808049	L1551/IRS5	67.892	18.13	K0c	2.430	I	1	–	Y	D07, C08
165	J04313613+1813432	LkHa358	67.901	18.23	K8	0.790	I	1	–	Y	W16
166	J04313747+1812244	HH30	67.906	18.21	M0	0.701	I	1	–	Y	B96
167	J04313843+1813576	HLTau	67.910	18.23	K7	0.801	I	1	–	N	
168	J04314007+1813571	XZTauA+B	67.917	18.23	M2	0.575	II	2	0.311	Y	L93, G93
169	J04314444+1808315	L1551NE	67.935	18.14	K0c	2.430	I	1	–	N	
170	J04315056+2424180	HKTauA+B	67.961	24.41	M0.5	0.667	II	2	2.4	Y	L93, S95, K11
171	J04315779+1821380	V710TauA	67.991	18.36	M0.5	0.667	II	2	3.24	Y	L93
172	J04315844+2543299	J1-665	67.993	25.72	M5.5	0.137	III	1	–	Y	L93, S95, K11
173	J04315968+1821305	LkHa267	67.999	18.36	M1.5	0.604	II	1	–	N	
174	J04320329+2528078	–	68.014	25.47	M6.25	0.086	III	1	–	Y	K12, T14
175	J04320926+1757227	L1551-51	68.039	17.96	K7	0.801	III	1	–	Y	K11
176	J04321456+1820147	V827Tau	68.061	18.34	K7	0.801	III	2	0.0929	Y	L93, K11
177	J04321540+2428597	Haro6-13	68.064	24.48	M0	0.701	II	1	–	Y	L93, G93, C08, K11
178	J04321583+1801387	V826TauA+B	68.066	18.03	K7	0.801	III	1	−1	Y	L93, S99, K11
179	J04321606+1812464	MHO5	68.067	18.21	M6	0.096	II	1	–	Y	K06, W16
180	J04321786+2422149	–	68.074	24.37	M5.75	0.116	III	1	–	Y	W16
181	J04321885+2422271	V928TauA+B	68.079	24.37	M0.5	0.667	III	2	0.22	Y	L93, G93, S95, K07, K12
182	J04322210+1827426	MHO6	68.092	18.46	M4.75	0.201	II	1	–	Y	W16
183	J04322329+2403013	–	68.097	24.05	M7.75	0.038	III	1	–	Y	K12, T14
184	J04322415+2251083	–	68.101	22.85	M4.5	0.225	II	1	–	N	
185	J04322627+1827521	MHO7	68.109	18.46	M5.25	0.157	III	1	–	Y	W16
186	J04323028+1731303	GGTauBa+Bb	68.126	17.53	M5.5	0.137	II	2	1.4	Y	L93
187	J04323034+1731406	GGTauAa+Ab	68.126	17.53	K7	0.801	II	3	0.288,0.0317	Y	L93, G93, S99, F14
188	J04323058+2419572	FYTau	68.127	24.33	K5	1.121	II	1	–	Y	L93, S95, K11
189	J04323176+2420029	FZTau	68.132	24.33	M0	0.701	II	1	–	Y	L93, G93, S95, K11
190	J04323205+2257266	IRAS 04295+2251	68.134	22.96	K7	0.801	I	1	–	Y	D07, C08
191	J04324303+2552311	UZTauA	68.179	25.88	M1	0.633	II	3	−1.,0.34,3.78	Y	L93, G93, S95, K11, D15
192	J04324373+1802563	L1551-55	68.182	18.05	K7	0.801	III	1	–	Y	S98, K11
193	J04324911+2253027	JH112	68.205	22.88	K6	0.906	II	4	0.66,1.52,6.4	Y	W16
194	J04325026+2422115	–	68.209	24.37	M7.5	0.044	III	1	–	N	
195	J04325119+1730092	LH0429+17	68.213	17.50	M8.25	0.026	III	1	–	N	
196	J04330197+2421000	MHO8	68.258	24.35	M6	0.096	III	2	0.037	Y	K06, K12, W16
197	J04330622+2409339	GHTauA+B	68.276	24.16	M2	0.575	II	2	0.314	Y	L93, G93, D15
198	J04330664+2409549	V807TauA+B	68.278	24.17	K5	1.121	II	3	0.023,0.41	Y	L93, G93, S95, D15
199	J04330781+2616066	KPNO14	68.283	26.27	M6	0.096	III	1	–	Y	K06
200	J04330945+2246487	–	68.289	22.78	M6	0.096	II	1	–	N	

Table C.1. continued.

#	2MASS	Name	RA_J2000	Dec_J2000	SpT	M [$M_\odot$]	Class	n_*	Sep [″]	HAR	HAR Ref.
201	J04331003+2433433	V830Tau	68.292	24.56	K7	0.801	III	2	6.95	Y	L93, S98, K11
202	J04331435+2614235	IRAS 04301+2608	68.310	26.24	M0	0.701	II	1	–	N	
203	J04331650+2253204	IRAS 04302+2247	68.319	22.89	M0c	0.701	I	1	–	Y	P99, C08
204	J04331907+2246342	IRAS 04303+2240	68.329	22.78	M0.5	0.667	II	1	–	Y	W16
205	J04332621+2245293	XEST17-036	68.359	22.76	M4	0.271	III	1	–	N	
206	J04333405+2421170	GITau	68.392	24.35	K7	0.801	II	1	–	Y	L93, G93, S95, K11
207	J04333456+2421058	GKTau	68.394	24.35	K7	0.801	II	2	2.5	Y	L93, G93, R93, S95, K11
208	J04333678+2609492	ISTauA+B	68.403	26.16	M0	0.701	II	2	0.221	Y	L93, G93, S95, D15
209	J04333905+2227207	–	68.413	22.46	M1.75	0.590	II	1	–	N	
210	J04333906+2520382	DLTau	68.413	25.34	K7	0.801	II	1	–	Y	L93, S95, K11
211	J04333935+1751523	HNTauA+B	68.414	17.86	K5	1.121	II	2	3.2	Y	L93, S99, K11, D15
212	J04334171+1750402	–	68.424	17.84	M4	0.271	II	1	–	N	
213	J04334291+2526470	–	68.429	25.45	M8.75	0.018	III	1	–	Y	K12, T14
214	J04334465+2615005	–	68.436	26.25	M4.75	0.201	II	1	–	N	
215	J04334871+1810099	DMTau	68.453	18.17	M1	0.633	II	1	–	Y	L93, K11
216	J04335200+2250301	CITau	68.467	22.84	K7	0.801	II	1	−1	Y	L93, G93, S95, K11
217	J04335245+2612548	–	68.469	26.22	M8.5	0.022	II	1	–	Y	K12
218	J04335252+2256269	XEST17-059	68.469	22.94	M5.75	0.116	III	1	–	N	
219	J04335470+2613275	ITTauA	68.478	26.22	K2	2.134	II	2	2.48	Y S95, K11	
220	J04335546+1838390	J2-2041	68.481	18.64	M3.5	0.335	III	2	0.418	Y	W16
221	J04341099+2251445	JH108	68.546	22.86	M1	0.633	III	1	–	Y	S95, K11
222	J04341527+2250309	CFHT1	68.564	22.84	M7	0.057	III	1	–	Y	K06
223	J04341803+1830066	HBC407	68.575	18.50	G8	2.562	III	2	0.13	Y	S98
224	J04344544+2308027	–	68.689	23.13	M5.25	0.157	III	1	–	Y	K12
225	J04345542+2428531	AATau	68.731	24.48	K7	0.801	II	1	–	Y	L93, S95, K11
226	J04345693+2258358	XEST08-003	68.737	22.98	M1.5	0.604	III	1	–	N	
227	J04350850+2311398	–	68.785	23.19	M6	0.096	III	1	–	Y	T14
228	J04352020+2232146	HOTau	68.834	22.54	M0.5	0.667	II	1	–	Y	S95, K11
229	J04352089+2254242	FFTauA+B	68.837	22.91	K7	0.801	III	2	0.0363	Y	L93, S95, K11
230	J04352450+1751429	HBC412A+B	68.852	17.86	M2	0.575	III	2	0.7	Y	L93
231	J04352737+2414589	DNTau	68.864	24.25	M0	0.701	II	1	–	Y	L93, S95, K11
232	-	IRAS 04325+2402C	68.897	24.14	M8c	0.031	II	1	–	N	
233	J04353539+2408194	IRAS 04325+2402A+B	68.897	24.14	M0c	0.701	I	1	–	N	
234	J04354093+2411087	CoKuTau3A+B	68.921	24.19	M1	0.633	II	2	2.04	Y	L93, S95, K11
235	J04354183+2234115	KPNO8	68.924	22.57	M5.75	0.116	III	1	–	Y	K06
236	J04354203+2252226	XEST08-033	68.925	22.87	M4.75	0.201	III	1	–	N	
237	J04354526+2737130	–	68.939	27.62	M9.25	0.013	III	1	–	Y	T14
238	J04354733+2250216	HQTau	68.947	22.84	K2	2.134	II	1	–	Y	S95
239	J04355109+2252401	KPNO15	68.963	22.88	M2.75	0.442	III	1	–	N	
240	J04355143+2249119	KPNO9	68.964	22.82	M8.5	0.022	III	1	–	Y	K06
241	J04355209+2255039	XEST08-047	68.967	22.92	M4.5	0.225	III	1	–	N	
242	J04355277+2254231	HPTau	68.970	22.91	K3	1.796	II	2	0.017	Y	L93, G93, S95, K11
243	J04355286+2250585	XEST08-049	68.970	22.85	M4.25	0.248	III	1	–	N	
244	J04355349+2254089	HPTau/G3	68.973	22.90	K7	0.801	III	2	0.022	Y	L93, G93, S95, K11
245	J04355415+2254134	HPTau/G2	68.976	22.90	G0	2.659	III	1	–	Y	L93, G93, S95, K11
246	J04355684+2254360	Haro6-28A+B	68.987	22.91	M3	0.398	II	2	0.66	Y	L93, S95
247	J04355892+2238353	XEST09-042	68.996	22.64	M0	0.701	III	1	–	N	
248	J04361030+2159364	–	69.043	21.99	M8.5	0.022	II	1	–	Y	T14
249	J04361038+2259560	CFHT2	69.043	23.00	M7.5	0.044	III	1	–	Y	K06
250	J04361909+2542589	LkCa14	69.080	25.72	M0	0.701	III	1	–	Y	L93, K11
251	J04362151+2351165	–	69.090	23.85	M5.25	0.157	II	1	–	N	
252	J04363893+2258119	CFHT3	69.162	22.97	M7.75	0.038	III	1	–	Y	K06
253	J04373705+2331080	–	69.404	23.52	L0	0.009	III	1	–	Y	T14
254	J04375670+2546229	ITG1	69.486	25.77	M5c	0.178	II	1	–	N	

Table C.1. continued.

#	2MASS	Name	RA_J2000	Dec_J2000	SpT	M [$M_\odot$]	Class	n_*	Sep [″]	HAR	HAR Ref.
255	J04380083+2558572	ITG2	69.503	25.98	M7.25	0.051	III	1	–	Y	K07, K12
256	J04381486+2611399	–	69.562	26.19	M7.25	0.051	II	1	–	N	
257	J04381630+2326402	–	69.568	23.44	M4.75	0.201	III	1	–	N	
258	J04382134+2609137	GMTau	69.589	26.15	M6.5	0.076	II	1	–	Y	K06, W16
259	J04382858+2610494	DOTau	69.619	26.18	M0	0.701	II	1	–	Y	L93, G93, S95, K11
260	J04383528+2610386	HVTauA+B	69.647	26.18	M1	0.633	III	3	0.036/4.00	Y	L93, S95, K11
261	J04385859+2336351	–	69.744	23.61	M4.25	0.248	II	1	–	Y	K12
262	J04385871+2323595	–	69.745	23.40	M6.5	0.076	III	1	–	Y	K12, T14
263	J04390163+2336029	–	69.757	23.60	M6	0.096	II	1	–	Y	K12
264	J04390396+2544264	–	69.767	25.74	M7.25	0.051	II	1	–	Y	T14
265	J04390525+2337450	–	69.772	23.63	M4c	0.271	I	1	–	N	
266	J04390637+2334179	–	69.777	23.57	M7.5	0.044	III	1	–	Y	K12, T14
267	J04391389+2553208	IRAS 04361+2547	69.808	25.89	K2c	2.134	I	1	–	Y	D07
268	J04391741+2247533	VYTauA+B	69.823	22.80	M0	0.701	II	2	0.66	Y	L93, S95
269	J04391779+2221034	LkCa15	69.824	22.35	K5	1.121	II	2	0.078	Y	L93, K11, K12
270	J04392090+2545021	GNTauA+B	69.837	25.75	M2.5	0.486	II	2	0.041	Y	S95
271	J04393364+2359212	–	69.890	23.99	M5	0.178	II	1	–	N	
272	J04393519+2541447	IRAS 04365+2535	69.897	25.70	K2c	2.134	I	1	–	Y	D07, C08
273	J04394488+2601527	ITG15	69.937	26.03	M5	0.178	II	1	–	N	
274	J04394748+2601407	CFHT4	69.948	26.03	M7	0.057	II	1	–	Y	K06
275	–	IRAS 04368+2557	69.974	26.05	K5c	1.121	0	1	–	N	
276	J04395574+2545020	IC2087IR	69.982	25.75	G5c	2.616	I	1	–	Y	C08
277	J04400067+2358211	–	70.003	23.97	M6	0.096	II	1	–	Y	D07, C08
278	J04400174+2556292	–	70.007	25.94	M5.5	0.137	III	2	0.575	Y	K07
279	J04400800+2605253	IRAS 04370+2559	70.033	26.09	M2c	0.575	II	1	–	N	
280	J04403979+2519061	–	70.166	25.32	M5.25	0.157	II	2	0.049	Y	K07, K12
281	J04404950+2551191	JH223	70.206	25.86	M2	0.575	II	2	2.1	Y	K11, W16
282	J04410424+2557561	Haro6-32	70.268	25.97	M5	0.178	III	1	–	Y	S95
283	J04410470+2451062	IWTauA+B	70.270	24.85	K7	0.801	III	2	0.27	Y	L93, S95
284	J04410826+2556074	ITG33A	70.284	25.94	M3	0.398	II	1	–	N	
285	J04411078+2555116	ITG34	70.295	25.92	M5.5	0.137	II	1	–	N	
286	J04411267+2546354	IRAS 04381+2540	70.303	25.78	M2c	0.575	I	1	–	Y	C08
287	J04411681+2840000	CoKuTau/4	70.320	28.67	M1.5	0.604	II	2	0.054	Y	I08
288	J04412464+2543530	ITG40	70.353	25.73	M3.5	0.335	II	1	–	N	
289	J04413882+2556267	IRAS 04385+2550	70.412	25.94	M0	0.701	II	1	–	Y	D07
290	J04414489+2301513	–	70.437	23.03	M8.5	0.022	II	2	0.108	Y	T10, T14
291	J04414565+2301580	–	70.440	23.03	M4.5	0.225	III	2	0.224	Y	T10, K11, T14
292	J04414825+2534304	–	70.451	25.58	M7.75	0.038	II	1	–	Y	T14
293	J04420548+2522562	LkHa332/G2A+B	70.523	25.38	M0	0.701	III	2	0.3	Y	L93
294	J04420732+2523032	LkHa332/G1A+B	70.531	25.38	M1	0.633	III	2	0.215	Y	L93, G93
295	J04420777+2523118	V955TauA+B	70.532	25.39	K7	0.801	II	2	0.33	Y	L93
296	J04422101+2520343	CIDA7	70.588	25.34	M4.75	0.201	II	1	–	Y	W16
297	J04423769+2515374	DPTau	70.657	25.26	M0.5	0.667	II	2	0.1067	Y	L93, K11
298	J04430309+2520187	GOTau	70.763	25.34	M0	0.701	II	1	–	Y	L93, K11
299	J04432023+2940060	CIDA14	70.834	29.67	M5	0.178	II	2	0.053	Y	W16
300	J04333278+1800436	–	68.387	18.01	M1	0.633	II	1	–	N	
301	J04333297+1801004	HD 28867A+C	68.387	18.02	B9	3.250	II	2	−1.,3.07	N	
302	J04442713+2512164	IRAS 04414+2506	71.113	25.20	M7.25	0.051	II	1	–	Y	K07, K12, T14
303	J04455129+1555496	HD 30171	71.464	15.93	G5	2.616	III	1	–	Y	K98, D15
304	J04455134+1555367	IRAS 04429+1550	71.464	15.93	M2.5	0.486	II	1	–	N	
305	J04464260+2459034	RXJ04467+2459	71.677	24.98	M4	0.271	III	2	0.051	Y	W16
306	J04465305+1700001	DQTau	71.721	17.00	M0	0.701	II	1	−1	Y	L93, S99, K11
307	J04465897+1702381	Haro6-37A	71.746	17.04	K7	0.801	II	3	0.33,2.7	Y	L93, D99
308	J04470620+1658428	DRTau	71.776	16.98	K5	1.121	II	1	–	Y	L93, G93, S99, K11

Table C.1. continued.

#	2MASS	Name	RA_*J*2000	Dec_*J*2000	SpT	M [$M_\odot$]	Class	n_*	Sep [$''$]	HAR	HAR Ref.
309	J04474859+2925112	DSTau	71.952	29.42	K5	1.121	II	1	–	Y	L93, K11
310	J04484189+1703374	–	72.175	17.06	M7	0.057	III	1	–	Y	T14
311	J04514737+3047134	UYAurA+B	72.947	30.79	M0	0.701	II	2	0.88	Y	L93, G93
312	J04520668+3047175	IRAS 04489+3042	73.028	30.79	M4	0.271	I	1	–	Y	D07
313	J04551098+3021595	GMAur	73.796	30.37	K7	0.801	II	1	–	Y	L93, K11
314	J04552333+3027366	–	73.847	30.46	M6.25	0.086	III	1	–	Y	K12, T14
315	J04553695+3017553	LkCa19	73.904	30.30	K0	2.430	III	1	–	Y	L93, K11
316	J04554046+3039057	–	73.919	30.65	M5.25	0.157	III	1	–	Y	K12
317	J04554535+3019389	–	73.939	30.33	M4.75	0.201	II	1	–	Y	K07
318	J04554582+3033043	ABAur	73.941	30.55	B9	3.250	II	1	–	Y	L97, K11
319	J04554757+3028077	–	73.948	30.47	M4.75	0.201	III	2	6.368	Y	K11, K12
320	J04554820+3030160	XEST26-052	73.951	30.50	M4.5	0.225	III	1	–	N	
321	J04554969+3019400	–	73.957	30.33	M6	0.096	II	2	0.056	Y	K12
322	J04555288+3006523	–	73.970	30.11	M5.25	0.157	III	1	–	Y	K12
323	J04555605+3036209	XEST26-062	73.984	30.61	M4	0.271	II	1	–	N	
324	J04555636+3049374	–	73.985	30.83	M5	0.178	III	1	–	N	
325	J04555938+3034015	SUAur	73.997	30.57	G2	2.632	II	1	–	Y	L93, G93, C04, K11
326	J04560118+3026348	XEST26-071	74.005	30.44	M3.5	0.335	II	1	–	N	
327	J04560201+3021037	HBC427	74.008	30.35	K5	1.121	III	2	−1.,0.0323	Y	L93, K11, S13
328	J04574903+3015195	–	74.454	30.26	M9.25	0.013	III	1	–	Y	K12, T14
329	J04584626+2950370	MWC480	74.693	29.84	A2	3.076	II	1	–	N	
330	J05030659+2523197	V836Tau	75.777	25.39	K7	0.801	II	1	–	Y	L93, S93, K11
331	J05044139+2509544	CIDA8	76.172	25.17	M3.5	0.335	II	1	–	Y	K11, W16
332	J05052286+2531312	CIDA9	76.345	25.53	K8	0.790	II	2	2.28	Y	K11, W16
333	J05061674+2446102	CIDA10	76.570	24.77	M4	0.271	III	2	0.083	Y	W16
334	J05062332+2432199	CIDA11	76.597	24.54	M3.5	0.335	II	2	0.0972	Y	K11, W16
335	J05064662+2104296	–	76.694	21.07	M5.25	0.157	III	1	–	Y	K12
336	J05071206+2437163	RX J05072+2437	76.800	24.62	K6	0.906	III	1	–	Y	K11, W16
337	J05074953+3024050	RWAurA+B	76.956	30.40	K3	1.796	II	3	0.120,1.39	Y	L93, G93, K11
338	J05075496+2500156	CIDA12	76.979	25.00	M4	0.271	II	1	–	Y	K11, W16

Table C.2. Catalog of the first nearest neighbor couples of stars.

# Couple	Star #A		Name (Star A)	n_{*A}	Class (Star A)	Star #B		Name (Star B)	n_{*B}	Class (Star B)	δ_P [AU]	n_{*P}	HAR[a]	WP [Conf.][b]
1	4		HBC360	1	III	5		HBC361	1	III	1 018	2	**	C
2	232		IRAS 04325+2402C	1	II	233		IRAS 04325+2402A+B	1	I	1 144	2	–	C
3	244		HPTau/G3	2	III	245		HPTau/G2	1	III	1 407	3	**	C [Y]
4	186		GGTauBa+Bb	2	II	187		GGTauAa+Ab	2	II	1 454	4	**	C [Y]
5	294		LkHa332/G1A+B	2	III	295		V955TauA+B	2	II	1 462	4	**	C [Y]
6	121		FVTauA+B	2	II	122		FVTau/cA+B	2	II	1 723	4	**	C [Y]
7	290		–	2	II	291		–	2	III	1 725	4	**	C [Y]
8	303		HD 30171	1	III	304		IRAS 04429+1550	1	II	1 814	2	*	C
9	206		GITau	1	II	207		GKTau	2	II	1 836	3	**	C [Y]
10	143		DHTauA+B	2	II	144		DITauA+B	2	III	2 120	4	**	C [Y]
11	300		–	1	II	301	S	HD 28867A+C	2	II	2 379	3	–	C
12	188		FYTau	1	II	189		FZTau	1	II	2 396	2	**	C [Y]
13	242		HPTau	2	II	244		HPTau/G3	2	III	2 423	4	**	[Y]
14	180		–	1	III	181		V928TauA+B	2	III	2 562	3	**	C
15	99		Haro6-5B	1	I	100		FSTauA+B	2	II	2 784	3	**	C [Y]
16	1		HBC358A+B+C	4	III	3		HBC359	1	III	2 888	5	*	C
17	11		IRAS 04108+2803A	1	I	12		IRAS 04108+2803B	1	I	2 963	2	*	C
18	197		GHTauA+B	2	II	198		V807TauA+B	3	II	3 048	5	**	C [Y]
19	167		HLTau	1	I	168		XZTauA+B	2	II	3 252	3	*	C [Y]
20	14		–	1	II	16	S	V773TauA+B	3	II	3 277	4	**	C [Y]
21	293		LkHa332/G2A+B	2	III	294		LkHa332/G1A+B	2	III	3 623	4	**	[Y]
22	171		V710TauA	2	II	173		LkHa267	1	II	3 914	3	*	C [Y]
23	52		DDTauA+B	2	II	53		CZTauA+B	2	II	4 218	4	**	C
24	86		IRAS 04181+2654B	1	I	87		IRAS 04181+2654A	1	I	4 393	2	**	C
25	155		ZZTau	2	II	156		ZZTauIRS	1	II	4 907	3	**	C
26	57		V892Tau	3	II	59		V410X-ray7	2	II	4 998	5	**	C
27	165		LkHa358	1	I	167		HLTau	1	I	5 028	2	*	
28	273		ITG15	1	II	274		CFHT4	1	II	5 186	2	*	C
29	17		FMTau	1	II	16	S	V773TauA+B	3	II	5 293	4	**	
30	241		XEST08-047	1	III	242		HPTau	2	II	5 870	3	*	
31	246		Haro6-28A+B	2	II	245		HPTau/G2	1	III	6 087	3	**	
32	217		–	1	II	219		ITTauA	2	II	6 223	3	**	C
33	124		KPNO13	1	II	122		FVTau/cA+B	2	II	6 353	3	**	
34	261		–	1	II	263		–	1	II	7 367	2	**	C
35	125		DGTauB	1	I	127		DGTau	1	II	7 485	2	**	C
36	84		–	1	II	86		IRAS 04181+2654B	1	I	7 572	2	**	
37	54		IRAS 04154+2823	1	I	55		V410X-ray2	1	II	7 740	2	–	C
38	317		–	1	II	321		–	2	II	7 886	3	**	C
39	182		MHO6	1	II	185		MHO7	1	III	8 412	2	**	C
40	60	S	Hubble4	2	III	62		CoKuTau/1	2	II	8 633	4	**	C
41	94		IRAM 04191+1522	1	0	98		IRAS 04191+1523A	2	I	8 763	3	*	C
42	49		V410Anon25	1	III	51		V410TauA+B+C	3	III	8 807	4	*	C

Notes. Amongst the first-nearest-neighbor couples of stars (A, B), the ultra wide Pairs (UWPs) are defined as *mutual* first nearest neighbors. Column 1: couple reference (this work). Columns 2–5 (Star A): the star reference (this work, see Table C.1), presence of a spectroscopic binary associated to the star/stellar system A ("S" means one spectroscopic binary, "SS" means two spectroscopic binaries), the common Name of the star A, n_{*A} the total number of stars, above the unity if the star is not single (spectroscopic binaries are counted as one component), the class of the (primary star). Columns 6–9 (Star B): the star reference (this work, see Table C.1), presence of a spectroscopic binary associated to the star/stellar system A ("S" means one spectroscopic binary, "SS" means two spectroscopic binaries), the common Name of the star B, n_{*B}: the total number of stars, above the unity if the star is not single (spectroscopic binaries are counted as one component), the class of the (primary star). Columns 10–11: the separation of the two stellar components A and B and their total number of stars as a (hierarchical) couple. Column 12: flag to indicate whether the each star A and B has been observed at high angular resolution (**), if only one component has been observed at HAR (*) or if none of them have been observed at HAR (no mark). Column 13: "C" indicates a ultra wide pair candidate since the couple are mutual nearest neighbours. The presence of an [Y], this couple has been confirmed as gravitationally bound binaries using astrometric and spectroscopic techniques as reported in the work of Kraus & Hillenbrand (2009b) who focused on binaries with separation less than 4200 AU. The delimitation of separation range in their study is marked by a single horizontal line in the table.

Table C.2. continued.

# Couple	Star #A		Name (Star A)	n_{*A}	Class (Star A)	Star #B		Name (Star B)	n_{*B}	Class (Star B)	δ_P [AU]	n_{*P}	HAR[a]	WP [Conf.][b]
43	284		ITG33A	1	II	285		ITG34	1	II	9 151	2	–	C
44	74		IRAS 04166+2706	1	I	75		[GKH94]41	1	I	9 581	2	–	C
45	21		MHO2	3	II	22		MHO3	2	II	9 939	5	**	C
46	211		HNTauA+B	2	II	212		–	1	II	11 155	3	*	C
47	166		HH30	1	I	165		LkHa358	1	I	11 350	2	**	
48	238		HQTau	1	II	243		XEST08-049	1	III	11 882	2	*	C
49	19		CWTau	1	II	14		–	1	II	12 270	2	**	
50	240		KPNO9	1	III	238		HQTau	1	II	12 571	2	**	
51	259		DOTau	1	II	260		HVTauA+B	3	III	12 717	4	**	C
52	221		JH108	1	III	222		CFHT1	1	III	13 218	2	**	C
53	95	S	RYTau	1	II	101		LkCa21	2	III	13 231	3	**	C
54	239		KPNO15	1	III	244		HPTau/G3	2	III	13 272	3	*	
55	23		FPTau	1	II	25		CXTau	1	II	14 677	2	**	C
56	265		–	1	I	263		–	1	II	15 900	2	*	
57	20		CIDA1	1	II	21		MHO2	3	II	16 343	4	**	
58	204		IRAS 04303+2240	1	II	205		XEST17-036	1	III	16 543	2	*	C
59	282		Haro6-32	1	III	284		ITG33A	1	II	16 999	2	*	
60	266		–	1	III	263		–	1	II	17 315	2	**	
61	275		IRAS 04368+2557	1	0	274		CFHT4	1	II	17 320	2	*	
62	236		XEST08-033	1	III	239		KPNO15	1	III	17 699	2	–	
63	319		–	2	III	320		XEST26-052	1	III	18 004	3	*	C
64	103		XEST11-078	1	I	105		–	1	II	18 176	2	*	C
65	145		KPNO5	1	III	144		DITauA+B	2	III	18 180	3	**	
66	200		–	1	II	204		IRAS 04303+2240	1	II	18 717	2	*	
67	65		V410X-ray6	1	II	62		CoKuTau/1	2	II	18 854	3	*	
68	58		LR1	1	II	51		V410TauA+B+C	3	III	18 928	4	*	
69	199		KPNO14	1	III	202		IRAS 04301+2608	1	II	18 991	2	*	C
70	258		GMTau	1	II	259		DOTau	1	II	19 124	2	**	
71	70		V819Tau	1	II	71		FRTau	1	II	19 440	2	*	C
72	323		XEST26-062	1	II	325		SUAur	1	II	20 418	2	*	C
73	315		LkCa19	1	III	317		–	1	II	21 018	2	**	
74	164		L1551/IRS5	1	I	169		L1551NE	1	I	21 028	2	*	C
75	73		IRAS 04166+2708	1	I	74		IRAS 04166+2706	1	I	21 131	2	-	
76	15		IRAS 04111+2800G	1	I	19		CWTau	1	II	21 518	2	*	
77	61		KPNO2	1	III	64		IRAS 04158+2805	1	I	22 288	2	*	C
78	214		–	1	II	217		–	1	II	22 935	2	*	
79	138		GVTauA+B	2	I	141		–	1	I	23 247	3	*	C
80	256		–	1	II	258		GMTau	1	II	23 835	2	*	
81	318		ABAur	1	II	320		XEST26-052	1	III	23 949	2	*	
82	67		V410X-ray5a	1	III	65		V410X-ray6	1	II	24 016	2	*	
83	194		–	1	III	196		MHO8	2	III	24 557	3	*	C
84	234		CoKuTau3A+B	2	II	232		IRAS 04325+2402C	1	II	25 019	3	*	
85	306	S	DQTau	1	II	307		Haro6-37A	3	II	25 112	4	**	C
86	327	S	HBC427	2	III	321		–	2	II	25 217	4	**	
87	56		V410X-ray4	1	III	58		LR1	1	II	25 350	2	–	
88	77		–	1	II	80		IRAS 04173+2812	1	II	25 454	2	*	C
89	24		XEST20-066	1	III	28		XEST20-071	1	III	26 069	2	–	C
90	45		V410X-ray3	2	III	47		V410Anon13	1	II	27 846	3	**	C
91	326		XEST26-071	1	II	319		–	2	III	27 860	3	*	
92	88		–	1	II	91		–	1	II	28 414	2	**	C
93	308		DRTau	1	II	306	S	DQTau	1	II	28 545	2	**	
94	176		V827Tau	2	III	173		LkHa267	1	II	31 518	3	*	
95	286		IRAS 04381+2540	1	I	288		ITG40	1	II	32 071	2	*	C
96	264		–	1	II	270		GNTauA+B	2	II	32 449	3	**	C

Table C.2. continued.

# Couple	Star #A		Name (Star A)	n_{*A}	Class (Star A)	Star #B		Name (Star B)	n_{*B}	Class (Star B)	δ_P [AU]	n_{*P}	HAR[a]	WP [Conf.][b]
97	146		IQTau	1	II	150		KPNO6	1	II	32 469	2	**	C
98	279		IRAS 04370+2559	1	II	275		IRAS 04368+2557	1	0	32 773	2	–	
99	29		CIDA2	2	III	28		XEST20-071	1	III	33 260	3	*	
100	296		CIDA7	1	II	294		LkHa332/G1A+B	2	III	33 303	3	**	
101	76		IRAS 04169+2702	2	I	75		[GKH94]41	1	I	33 371	3	*	
102	9		LkCa1	1	III	10		Anon1	2	III	33 561	3	*	C
103	142		XEST13-010	1	III	138		GVTauA+B	2	I	34 032	3	*	
104	42		LkCa5	2	III	44		V410X-ray1	1	II	34 758	3	**	C
105	31		–	1	III	33		IRAS 04125+2902	1	II	34 814	2	*	C
106	311		UYAurA+B	2	II	312		IRAS 04489+3042	1	I	34 823	3	**	C
107	97		TTauN+S	3	II	102		–	1	III	34 836	4	**	C
108	140		IRAS 04264+2433	1	I	142		XEST13-010	1	III	35 413	2	–	
109	316		–	1	III	323		XEST26-062	1	II	36 423	2	*	
110	90		IRAS 04187+1927	1	II	97		TTauN+S	3	II	36 639	4	**	
111	68		FQTauA+B	2	II	70		V819Tau	1	II	37 298	3	**	
112	175		L1551-51	1	III	178	S	V826TauA+B	1	III	38 164	2	**	C
113	216	S	CITau	1	II	221		JH108	1	III	38 176	2	**	
114	272		IRAS 04365+2535	1	I	270		GNTauA+B	2	II	38 645	3	**	
115	35		–	1	II	36		–	1	III	38 905	2	**	C
116	108		–	1	II	109		IRAS 04200+2759	1	II	39 026	2	*	C
117	208		ISTauA+B	2	II	217		–	1	II	39 336	3	**	
118	136		J1-507	2	III	143		DHTauA+B	2	II	39 613	4	**	
119	231		DNTau	1	II	234		CoKuTau3A+B	2	II	41 386	3	**	
120	27		FOTauA+B	2	II	29		CIDA2	2	III	43 010	4	**	
121	195		LH0429+17	1	III	186		GGTauBa+Bb	2	II	43 406	3	*	
122	92		–	1	III	99		Haro6-5B	1	I	43 701	2	**	
123	314		–	1	III	319		–	2	III	44 092	3	**	
124	229		FFTauA+B	2	III	236		XEST08-033	1	III	44 299	3	*	
125	106		XEST11-087	1	III	107		IRAS 04196+2638	1	II	44 896	2	–	C
126	228		HOTau	1	II	235		KPNO8	1	III	45 051	2	**	C
127	89		XEST21-026	1	III	96		HD 283572	1	III	46 718	2	*	C
128	153		DKTauA	2	II	157		KPNO7	1	II	46 782	3	**	C
129	78		–	1	II	80		IRAS 04173+2812	1	II	47 540	2	*	
130	276		IC2087IR	1	I	272		IRAS 04365+2535	1	I	47 708	2	**	
131	120		–	1	II	123		IRAS 04239+2436	2	I	49 200	3	**	C
132	190		IRAS 04295+2251	1	I	193		JH112	4	II	49 520	5	**	C
133	247		XEST09-042	1	III	235		KPNO8	1	III	49 607	2	*	
134	218		XEST17-059	1	III	216	S	CITau	1	II	49 952	2	*	
135	148		–	1	II	142		XEST13-010	1	III	50 555	2	*	
136	184		–	1	II	193		JH112	4	II	50 864	5	*	
137	278		–	2	III	274		CFHT4	1	II	51 265	3	**	
138	281		JH223	2	II	285		ITG34	1	II	51 711	3	*	
139	249		CFHT2	1	III	246		Haro6-28A+B	2	II	51 901	3	**	
140	210		DLTau	1	II	213		–	1	III	52 147	2	**	C
141	313		GMAur	1	II	314		–	1	III	52 223	2	**	
142	297		DPTau	2	II	296		CIDA7	1	II	52 257	3	**	
143	271		–	1	II	277		–	1	II	52 540	2	*	C
144	203		IRAS 04302+2247	1	I	193		JH112	4	II	53 048	5	**	
145	132		L1521F-IRS	1	I	135		IRAS 04260+2642	1	II	53 092	2	–	C
146	224		–	1	III	227		–	1	III	53 928	2	**	C
147	289		IRAS 04385+2550	1	II	285		ITG34	1	II	53 990	2	*	
148	170		HKTauA+B	2	II	180		–	1	III	54 967	3	**	
149	177		Haro6-13	1	II	181		V928TauA+B	2	III	55 358	3	**	
150	30		KPNO1	1	III	24		XEST20-066	1	III	56 296	2	*	
151	192		L1551-55	1	III	178	S	V826TauA+B	1	III	56 740	2	**	

Table C.2. continued.

# Couple	Star #A		Name (Star A)	n_{*A}	Class (Star A)	Star #B		Name (Star B)	n_{*B}	Class (Star B)	δ_P [AU]	n_{*P}	HAR[a]	WP [Conf.][b]
152	252		CFHT3	1	III	249		CFHT2	1	III	57 088	2	**	
153	111		FUTauA	2	II	112		FTTau	1	II	57 650	3	*	C
154	226		XEST08-003	1	III	229		FFTauA+B	2	III	58 221	3	*	
155	298		GOTau	1	II	297		DPTau	2	II	62 261	3	**	
156	179		MHO5	1	II	176		V827Tau	2	III	62 832	3	**	
157	158		JH56	1	II	163		–	1	III	62 994	2	**	C
158	34		–	1	II	36		–	1	III	63 355	2	*	
159	129		KPNO4	1	III	127		DGTau	1	II	65 694	2	**	
160	159		MHO9	1	III	165		LkHa358	1	I	67 348	2	**	
161	41		CYTau	1	II	43		KPNO10	1	II	67 562	2	**	C
162	162		MHO4	1	III	164		L1551/IRS5	1	I	67 886	2	**	
163	110		–	1	II	107		IRAS 04196+2638	1	II	68 929	2	–	
164	267		IRAS 04361+2547	1	I	270		GNTauA+B	2	II	71 078	3	**	
165	152		FXTauA+B	2	II	148		–	1	II	78 616	3	**	
166	79		–	1	II	84		–	1	II	80 665	2	**	
167	66		KPNO12	1	II	64		IRAS 04158+2805	1	I	80 679	2	*	
168	26	SS	LkCa3A+B	2	III	30		KPNO1	1	III	80 734	3	**	
169	81		–	1	II	78		–	1	II	81 682	2	*	
170	2		XEST06-006	1	III	3		HBC359	1	III	81 920	2	–	
171	131		IRAS 04248+2612	3	I	129		KPNO4	1	III	81 988	4	**	
172	215		DMTau	1	II	301	S	HD 28867A+C	2	II	83 201	3	*	
173	253		–	1	III	257		–	1	III	84 385	2	*	C
174	220		J2-2041	2	III	223		HBC407	2	III	84 645	4	**	C
175	262		–	1	III	257		–	1	III	84 763	2	*	
176	116		J1-4423	1	III	117		IPTau	1	II	88 546	2	*	C
177	115		IRAS 04216+2603	1	II	118		J1-4872A	4	III	89 284	5	*	C
178	292		–	1	II	288		ITG40	1	II	90 553	2	*	
179	324		–	1	III	316		–	1	III	92 995	2	*	
180	85		–	1	II	93		DETau	1	II	93 845	2	*	C
181	255		ITG2	1	III	258		GMTau	1	II	94 578	2	**	
182	139		FWTauA+B+C	3	III	146		IQTau	1	II	94 593	4	**	
183	38		LkCa4	1	III	35		–	1	II	96 679	2	**	
184	322		–	1	III	315		LkCa19	1	III	97 217	2	**	
185	183		–	1	III	197		GHTauA+B	2	II	98 944	3	**	
186	82		XEST16-045	1	III	76		IRAS 04169+2702	2	I	99 191	3	*	
187	6		IRAS 04016+2610	1	I	2		XEST06-006	1	III	100 935	2	*	
188	334		CIDA11	2	II	336		RX J05072+2437	1	III	101 912	3	**	C
189	201		V830Tau	2	III	194		–	1	III	103 966	3	*	
190	254		ITG1	1	II	255		ITG2	1	III	105 891	2	*	
191	114		–	1	II	116		J1−4423	1	III	105 901	2	*	
192	32		–	1	II	29		CIDA2	2	III	106 340	3	*	
193	137		IRAS 04263+2654	2	II	135		IRAS 04260+2642	1	II	108 012	3	*	
194	172		J1-665	1	III	191	S	UZTauA	3	II	113 364	4	**	C
195	7		HBC362	1	III	5		HBC361	1	III	116 288	2	*	
196	333		CIDA10	2	III	334		CIDA11	2	II	116 916	4	**	
197	161		V927TauA+B	2	III	170		HKTauA+B	2	II	123 803	4	**	
198	18		FNTau	1	II	17		FMTau	1	II	127 248	2	**	
199	133		–	2	II	137		IRAS 04263+2654	2	II	128 758	4	**	
200	174		–	1	III	172		J1-665	1	III	129 422	2	**	

Table C.2. continued.

# Couple	Star #A	Name (Star A)	n_{*A}	Class (Star A)	Star #B		Name (Star B)	n_{*B}	Class (Star B)	δ_P [AU]	n_{*P}	HAR[a]	WP [Conf.][b]
201	225	AATau	1	II	231		DNTau	1	II	131 827	2	**	
202	72	LkCa7A+B	2	III	66		KPNO12	1	II	132 054	3	**	
203	40	–	1	II	33		IRAS 04125+2902	1	II	139 651	2	*	
204	50	KPNO11	1	III	72		LkCa7A+B	2	III	142 579	3	*	
205	119	KPNO3	1	II	118		J1-4872A	4	III	145 196	5	**	
206	113	–	1	II	110		–	1	II	146 597	2	*	
207	151	–	1	III	161		V927TauA+B	2	III	151 345	3	**	
208	149	UXTauA+C	4	II	159		MHO9	1	III	152 590	5	**	
209	209	–	1	II	205		XEST17-036	1	III	154 420	2	–	
210	280	–	2	II	293		LkHa332/G2A+B	2	III	165 802	4	**	
211	147	–	1	III	149		UXTauA+C	4	II	167 075	5	*	
212	251	–	1	II	233		IRAS 04325+2402A+B	1	I	168 337	2	–	
213	13	IRAS 04108+2910	1	II	31		–	1	III	171 241	2	*	
214	302	IRAS 04414+2506	1	II	298		GOTau	1	II	173 274	2	**	
215	250	LkCa14	1	III	254		ITG1	1	II	186 829	2	*	
216	126	DFTauA+B	2	II	125		DGTauB	1	I	194 340	3	**	
217	310	–	1	III	308		DRTau	1	II	196 526	2	**	
218	154	IRAS 04278+2253A+B	1	I	184		–	1	II	196 707	2	–	
219	331	CIDA8	1	II	332		CIDA9	2	II	197 874	3	**	C
220	328	–	1	III	327	S	HBC427	2	III	199 912	3	**	
221	230	HBC412A+B	2	III	212		–	1	II	205 652	3	*	
222	338	CIDA12	1	II	336		RXJ05072+2437	1	III	209 691	2	**	
223	330	V836Tau	1	II	331		CIDA8	1	II	212 426	2	**	
224	48	HBC372	1	III	63		HBC376	1	III	214 489	2	**	C
225	268	VYTauA+B	2	II	269		LkCa15	2	II	225 390	4	**	C
226	160	–	1	III	151		–	1	III	229 015	2	**	
227	329	MWC480	1	II	328		–	1	III	232 165	2	*	
228	283	IWTauA+B	2	III	280		–	2	II	239 911	4	**	
229	305	RXJ04467+2459	2	III	302		IRAS 04414+2506	1	II	280 537	3	**	
230	248	–	1	II	228		HOTau	1	II	290 923	2	**	
231	69	BPTau	1	II	40		–	1	II	294 777	2	**	
232	130	–	1	III	151		–	1	III	304 098	2	**	
233	83	J2-157	1	III	63		HBC376	1	III	312 079	2	**	
234	104	–	1	III	115		IRAS 04216+2603	1	II	330 781	2	*	
235	134	–	1	II	133		–	2	II	345 964	3	**	
236	299	CIDA14	2	II	309		DSTau	1	II	506 030	3	**	C
237	46	V409Tau	1	II	104		–	1	III	526 157	2	*	
238	287	CoKuTau/4	2	II	299		CIDA14	2	II	553 244	4	**	
239	237	–	1	III	158		JH56	1	II	553 251	2	**	
240	128	–	1	III	154		IRAS 04278+2253A+B	1	I	574 507	2	*	
241	8	–	2	III	9		LkCa1	1	III	575 274	3	*	
242	39	–	1	III	13		IRAS 04108+2910	1	II	717 882	2	–	
243	37	–	1	III	90		IRAS 04187+1927	1	II	909 525	2	**	
244	337	RWAurA+B	3	II	329		MWC480	1	II	1 026 057	4	*	
245	335	–	1	III	334		CIDA11	2	II	1 746 426	3	**	